TEAMER
Testing & Expertise for Marine Energy

Post Access Report

Tidal Current Turbine Parametric Study

Awardee: Hydrokinetic Energy Corp.

Awardee point of contact: Walter Schurtenberger

Facility: American Bureau of Shipping

Facility point of contact: Shirlyn Zhang

Date: July 31, 2022

EXECUTIVE SUMMARY

In this study, different variates of the original geometry of the current turbine designed by Hydrokinetic Energy Corp. (HEC) were evaluated for energy efficiency using Computational Fluid Dynamics (CFD). The objective was accomplished by a parametric study of the key geometric parameters for the shroud, the diffuser, and the hub. With the key parameters selected, a computer script was used to automatically generate the three-dimensional geometry file for CFD. A robust CFD model and gridding strategy were established based on ABS' internal best practices and a dedicated grid-size time-step convergence testing prior to the application of the setup to more than 100 study cases. From the CFD simulation results, it was found that the key to improving energy output of the current turbine is to reduce the obstruction of the turbine structures to the main flow. Among baseline designs with different numbers of blades, the 3-bladed one was found to be the most energy efficient. Among all 3-bladed design variates, a reduced thickness, a reduced maximum camber, and a maximum camber location moved downstream of the cross-sectional profile will result in an increased power output of the turbine. Compared to the baseline case, the design variate considered in the present study accomplished a 15% increase in power output. These findings revealed a pathway for the improvement of the turbine energy efficiency. The present parametric study will also lay the groundwork for a more sophisticated design optimization in future phases.

1 INTRODUCTION TO THE PROJECT

Hydrokinetic Energy Corp. (HEC, the Applicant) is developing an in-stream horizontal axis, axial flow turbine. This turbine is a shrouded or enclosed concept. HEC has designed a unique combination of rotor - hub - shroud - diffuser - excluder hydrofoil shapes to achieve flow acceleration through the rotor section of turbine. The principle is to apply the Bernoulli/Venturi effect to augment flow-through velocity. This flow acceleration, not yet seen in other commercially available turbines, is achieved by creating a negative pressure field on the downstream side of the turbine which in turn pulls the water through the rotor section at a higher velocity. This turbine concept is dynamic, can be scaled up or down and lends itself to usage in any kind of flowing water. HEC's proprietary Flow Acceleration Technology makes these turbines ideally suited for low-flow velocity environments of 0.75 m/s where other Hydrokinetic turbines are not capable of generating electricity.

HEC has designed several different variations of its patented concept with varying number of blades and varying profiles of shroud - diffuser – hub combination. Some of these design variations are ideally suited for low-flow velocity environments and enable the HEC concept to generate energy where conventional hydrokinetic turbines cannot produce. Low-flow velocity environment markets is what HEC would like to explore and exploit much more with its unique turbine concept.

This project will be assisted by the Facility, American Bureau of Shipping (ABS), with the optimization of the turbine geometry using Computational Fluid Dynamics (CFD). With the proposed budget, the optimization will be accomplished by a parametric study of the key geometric parameters for the blade, the shroud, the diffuser, and the hub. The objective is the maximization of the power coefficient of the turbine. Throughout the project period, HEC will provide technical guidance in terms of the acceptance criteria of the turbine power performance, the allowable ranges of the geometrical parameters, and the interpretation of the CFD results from the design perspective. Unlike a global optimization of a design which searches for an optimal solution by a sophisticated algorithm, our proposed parametric study only involves CFD calculation of the hydrodynamic performance of each pre-determined variate of the baseline design. This approach is not expected to lead to an exact optimal solution, but it will provide invaluable insight into the directions for design modification. In a future phase, a full optimization guided by search algorithms can be attempted based on what has been learned from the present project.

2 ROLES AND RESPONSIBILITIES OF PROJECT PARTICIPANTS

2.1 APPLICANT RESPONSIBILITIES AND TASKS PERFORMED

HEC will provide the complete 3D models of two different design options of the accelerator shroud, diffuser, and open center hub, all of which are of the same prototype size. The baseline design for the present study will be selected from these two design options. Along with the design options, HEC will also provide three different rotor sections. There will be a three-bladed option, a four-bladed option, and a five-bladed option. Additionally, HEC will provide two different current flow profiles which can be used to compare the results in two different flow environments.

HEC can provide more design profiles of the accelerator shroud, diffuser, and hub as deemed necessary

by ABS. HEC will also support ABS in the form of 3D design work when necessary while the project is ongoing.

Throughout this project, there will be frequent communications between the two parties mostly in the form of virtual meetings to discuss the numerical results as they become available.

2.2 Network Facility Responsibilities and Tasks Performed

ABS, as the network facility, will provide parametric study using CFD, deliver results summary and recommendations to the Applicant. ABS' key tasks are as follows:

- Discuss with the Applicant about the baseline design, parameterization approach, parameter constraints, and objective function
- Set up a CFD model for the 4-blade baseline design
    - Conduct CFD model time-step and grid convergence testing
    - Generate performance curve for the baseline design
- Identify the optimal number of turbine blades (from 3-, 4-, and 5-blade designs)
- Vary the key parameters for the shroud and run CFD for each variate
    - Identify the best shroud design
- Vary the key parameters for the diffuser and run CFD for each variate
    - Identify the best diffuser design
- Vary the key parameters for the hub and run CFD for each variate
    - Identify the best hub design
- Assuming that the optimal design consists of the best shroud – diffuser – hub components, generate performance curve for the optimal design
- Report findings

3 Project Objectives

HEC's long-term objective is to design an array of riverine/tidal energy harvesting turbines for maximal power output, for which design optimization of a single turbine will be critical. In this project, HEC aims to test different geometrical configurations of a single turbine using high-fidelity CFD modeling. The specific technical assistance objectives are as follows:

1. To parameterize a turbine's geometrical configuration for further parametric studies, e.g., the number of turbine blades; the section profiles of the shroud, diffuser, and hub; the diameter and expansion of the diffuser.
2. To determine an optimal turbine design/configuration with the maximum power output.

This project will focus on the hydrodynamic performance of the turbine in a river/tidal channel. The key performance indicators will include

- Flow volume rate through the rotor plane
- The maximum torque coefficient for the design
- The maximum power coefficient for the design

The optimization of the turbine design will have a large influence on the LCOE of these turbines later in

production. The increased volumetric flow rate by using flow accelerating devices will increase the rotor RPM, augment the torque and energy extracted which will lower the LCOE. It is anticipated that by modifying the geometries the efficiency of this turbine design can be increased to a level of 10% to 30% higher than that of the traditional hydrokinetic turbines depending on the increased flow velocity available. It is known that the percentage increase in efficiency is not a linear progression, but will follow an exponential relation with the doubling or tripling of the ambient flow velocity.

4 Test Facility, Equipment, Software, and Technical Expertise

- **Overall expertise of ABS**

ABS is a not-for-profit marine classification, standards, and technology organization in the U.S. ABS has over 3,000 engineers, scientists, and marine surveyors with global expertise related to the design, installation, operation, and maintenance of marine and offshore assets. ABS has 10-15 research projects per year on CFD application to ship and offshore topics (e.g., wave and current loads on marine structures/assets).

- **Simulation and data analysis software**

ABS has expert-level skills at general CFD software such as OpenFOAM and Star-CCM+. For the present project, ABS will use OpenFOAM (also referred to as "ABSFoam"), which has been enhanced and secondary-developed for marine and offshore applications. Hexpress (NUMECA International) will be used for mesh generation. CFD post-processing or visualization is implemented by Paraview. Data analysis will be carried out by numerous Python scripts developed for routine CFD needs.

- **Simulation hardware**

ABS has its in-house High-Performance Computing (HPC) hardware, including three clusters with a total of more than 1,000 cores. ABS HPC is managed daily by a professional IT team that supports the entire company.

- **ABS key personnel expertise**

ABS' numerical simulation work will be managed by Dr. Zhongfu Ge, Manager of Technology, and supported by a Senior CFD Engineer. Dr. Ge has been leading ABS' global CFD capabilities for more than five years and has extensive experience in solving industrial problems using CFD as well as project management. The ABS team has experience in similar projects (CFD analysis for ducted water turbines), which assures success for the present project.

5 Test or Analysis Article Description

The Flow Acceleration Technology (FAT) that HEC has developed is based on the Bernoulli/Venturi effect. The hydrofoil shapes of the accelerator shroud, diffuser and the open center hub create a low-pressure area on the downstream side of the turbine. This low-pressure field downstream pulls the water through the rotor section at a higher speed than the ambient flow velocity. This accelerated flow velocity through

the rotor section increases the RPM of the rotor allowing augmented extraction of torque and energy. HEC believes that this feature is unique and makes the HEC turbine well suited for operation in low flow velocity environments.

To HEC's knowledge, there are no commercial Hydrokinetic turbines available that function in flow velocities below 1 m/s or 2 knots to extract energy efficiently. Based on HEC's tank testing, the turbine design considered here is well suited for applications with low/variable tidal flows. Figure 1 shows a preliminary model in HEC's test tank.

Figure 1. Preliminary model in HEC's test tank.

HEC envisions that the optimization of this turbine geometry will lead to an advancement in current energy converters and once commercially available this could make a socio-economic impact.

6 Work Plan

6.1 Numerical Model Description

ABS will use a high-fidelity CFD model based on 3D Reynolds-Averaged Navier-Stokes (RANS) equations, supplemented by a $k-\omega$ SST turbulence model. The governing equations will be discretized by the Finite Volume Method. The computational domain will consist of unstructured grids, with various refinement zones for the areas where flow properties are expected to change rapidly. Viscous layers (or prism layers) will be generated around solid walls to resolve boundary layers. Wall functions will be used for calculating the flow dynamics in the boundary layers. A dynamic rotating grid will be created for the rotor (turbine blades and the hub) domain, which is assembled with the stationary background domain. The simulation will be unsteady. We will monitor time histories of the total thrust and total torque of the rotor until they reach a steady, oscillatory state.

ABS will use OpenFOAM as the CFD platform, which has been enhanced and secondary-developed for marine and offshore applications (informally referred to as "ABSFoam"). Hexpress will be used for mesh generation. CFD post-processing is partially done within the OpenFOAM model and partially implemented with a separate software tool, Paraview. All flow visualization is performed by Paraview.

For the time-step and grid-size convergence testing, a matrix of two different grid-size levels (for example, fine and medium) by two different time-step levels will be used for the baseline design. The best grid-size

and time-step strategy will be determined to achieve economy and converged accuracy. Moreover, as the parametric study will involve very small changes in the geometries, the use of consistent computational grids will be critical. We plan to only make local changes to the grids for each design. The overall grid structure should remain as consistent as possible across different designs.

In addition to the dedicated time-step and grid-size testing, ABS has conducted numerous validation studies in the past years. As propeller performance, ducted or not, is a major strength in ABS' core expertise, CFD model validation against experimental results has been thoroughly conducted and well-documented for propellers. For this particular project, CFD results can also be compared with existing results obtained by the Applicant using different numerical tools. Such cross-code comparison will help increase confidence in the CFD results.

6.2 Test and Analysis Matrix and Schedule

The CFD-based parametric study will focus on the variation of the shroud, the diffuser, and the hub geometries. These three geometries are all revolved bodies. Optimization of each will be realized by the variation of their respective cross sections. With the limited budget, we will defer the variation of the turbine blades to future projects. That means we are not planning to vary the diameter of the hub or the diameter of the shroud.

Before detailed variations of the geometries, we first understand that the number of the turbine blades will have significant effects on the turbine power performance. For this reason, a performance comparison (indicated by the power coefficient, C_p) will be made for the baseline design with three, four, and five blades. The number of blades that results in the highest power coefficient will proceed to all subsequent steps regarding section optimization.

The cross sections of the shroud, the diffuser, and the hub, are similar to a NACA airfoil. Such sectional profiles can be characterized by four parameters: chord length, thickness, camber, and the maximum camber location; see Figure 2 as an example. This approach will be applicable to the shroud, the diffuser, and the hub. In addition, the diffuser will have one additional parameter, which is the expansion ratio. Therefore, there will be a total of 10 parameters for describing the three geometrical parts:

- Shroud: thickness, camber, and the maximum camber location (chord length is omitted as it is judged not critical for increasing flow rate)
- Hub: thickness and camber (others omitted for simplicity)
- Diffuser: thickness, camber, and the maximum camber location, diameter, and expansion ratio (chord length is omitted for simplicity)

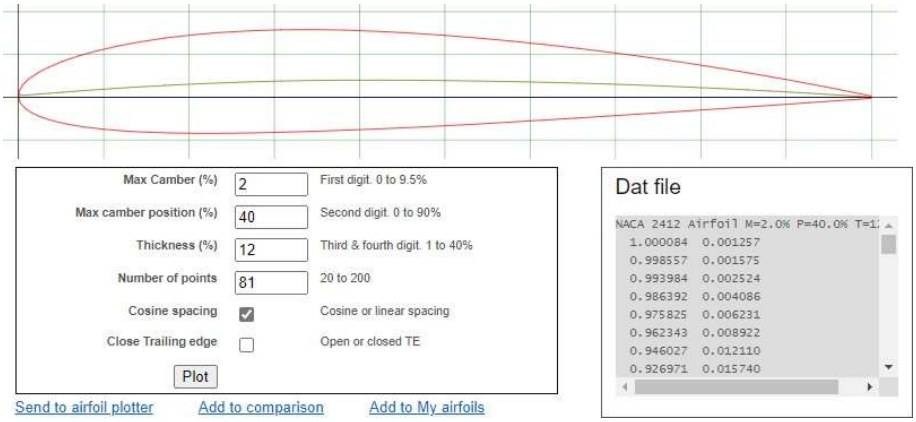

Figure 2. Generation of the NACA four-digit airfoils (Source: *airfoiltools.com*)

For this phase of development, we are not aiming to do a full-blown optimization with advanced search algorithms. For the limited time and budget, ABS will carry out a simplified parametric study in order to identify the general direction for improving power output. The best design identified in the end will not necessarily be the global optimal design in a broad sense. However, the results should be able to show the correct directions for improvement.

In the present project, we will run through a pre-set matrix of design variables and compare between designs. Even so, the design matrix will be prohibitively large. In order to further simplify the analysis, we assume that the three parts, i.e., the shroud, the diffuser, and the hub, can be optimized independently (see Figure 3 for this idea). This is reasonable since the small changes in the sectional profile of one part will only affect the flow in its own vicinity but will not significantly affect that of the other parts farther away.

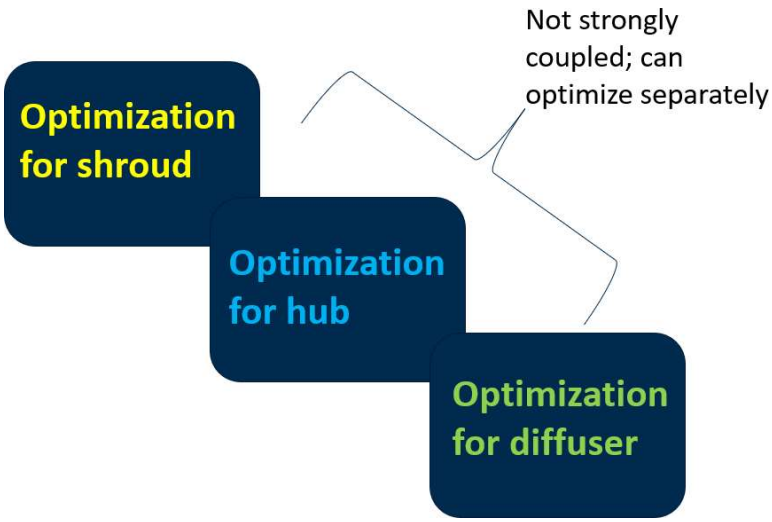

Figure 3. The three parts of the current turbine are not closely correlated to one another; as a result, they can be optimized in order separately.

A second assumption we make to simplify the analysis is that it is only necessary to compare the changes

in the power coefficient at the peak RPM (or equivalently, the peak Tip Speed Ratio, TSR) rather than at the entire RPM range (see Figure 4 for illustration). We assume that by tuning the design parameters the overall power output curve will be elevated or depressed but will not shift along the RPM axis significantly. This assumption will help avoid the assessment of the entire power coefficient curve for every design.

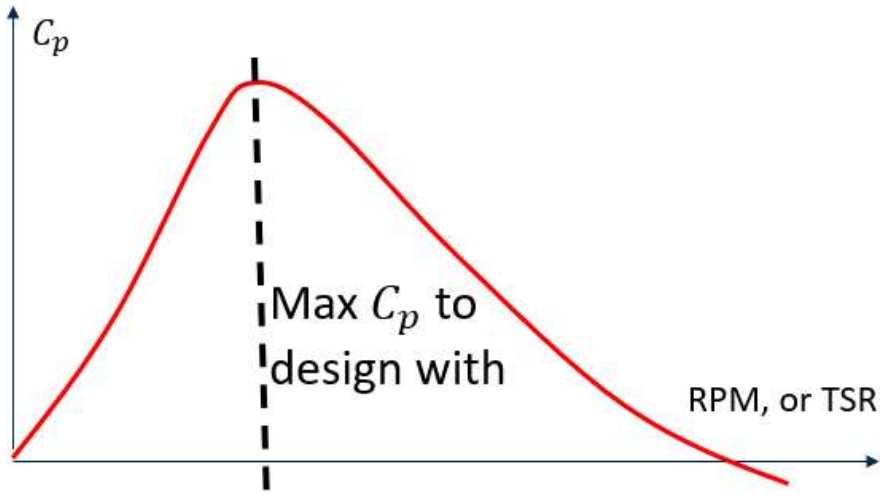

Figure 4. The peak RPM as defined by the maximum power coefficient of the baseline design will be used for evaluating different designs.

A third assumption we make is when varying a certain design parameter we only vary it by ±10% of the value of the baseline design. It is understood that HEC's baseline design is not a random configuration but already a modified version based on previous studies. The variation of ±10% will help show the directions for further improvement. The determination of the exact increment or decrement of all parameters is only possible with a sophisticated optimization, which is out of the scope of the present project.

Finally, we also assume that the order of importance of the three parts for flow acceleration is the shroud, the diffuser, and the hub, from high to low. The separate part optimization will follow the same order.

Following the reasoning above, we present a more specific test plan and the proposed schedule as follows. During the project execution, some designs/cases could be omitted if similar designs show negligible improvement of the flow conditions. The decision on omitting any case will be proposed by ABS and agreed to by HEC. This flexibility is allowed due to the large number of cases planned.

At the end of stages C, D, E, and F in Table 1 shown below, a best design up to that point will be recommended and enter the next stage. ABS will seek agreement from HEC on the recommended design.

Table 1. The tasks for CFD simulations on various stages.

Stage	Task	Number of cases	Time cost (week)	Note
A. Grid-size time-step convergence test	Test baseline design with a 3x3 grid-size and time-step matrix	N/A	1	The best setup will proceed to next stages
B. Baseline Power curve	Run 8 RPMs for the baseline design	8	0.8	Find the peak RPM for all subsequent cases
C. Best number of blades	Compare 3, 4, 5 blade design for baseline	2	0.2	Fix number of blades for subsequent steps
D. Modify shroud	3 cambers, 3 thicknesses, 3 maximum camber locations	27	3	Only best one proceeds to next steps
E. Modify diffuser	3 cambers, 3 thicknesses, 3 maximum camber locations, 2 diameters, 2 expansions	108	7	Only best one proceeds to next steps
F. Modify hub	3 cambers, 3 thicknesses	9	1	Identify the best design
G. Final power curve	Run 7 more RPMs for the best design	7	1	
H. Reporting	Final report		1	
Total		161	15	

6.3 Safety

The mission of ABS is to serve the public interest as well as the needs of our clients by promoting the security of life and property and preserving the natural environment. ABS is committed to excellence in environmental, health and safety management. ABS promotes a safe and healthy environment for staffs and visitors, through programs and practices designed to protect people and the environment.

The ABS staffs will follow all relevant safety procedures and protocols outlined on the ABS Health, Safety, Quality, Environmental (HSQE) SharePoint Site (internal access only).

In early 2020, ABS became increasingly concerned with enforcing sanitization of the office space to protect employees from COVID-19. Between March 2020 and February 2022, ABS employees worked from home. ABS project engineers had remote access to the server to run the numerical analysis. Since all proposed work will be performed on the computer, the safety risks for the project will be minimal.

6.4 Contingency Plans

- **Manpower**

ABS will have at least three qualified CFD modelers who can support the proposed project during the project time. The manpower will be more than sufficient to carry out the project to completion.

- **Schedule**

The project is budgeted for 600 man-hours based on ABS' rates and the budget requested. If the project is to be executed by one staff member full time, the project should be completed within 15 weeks, which is about 4 months. As requested by the Applicant, ABS will plan to complete this project before the end of this year. We have extra manpower to shorten the project period to be less than four months (till the end of the year).

- **Computation hardware**

ABS has its in-house HPC resources. In the very rare scenario where internal resources become unavailable, ABS will use external resources such as those from the Texas Advanced Computing Center (TACC). ABS has an existing account with TACC and has used their service before. ABS will be responsible for any extra cost for using TACC.

6.5 Data Management, Processing, and Analysis

6.5.1 Data Management

During the project, ABS will provide a secure data management environment for collaborative work among project team members. Our team will store and maintain the data in the Microsoft (MS) Teams environment with integrated MS Office applications. Microsoft OneDrive will be used to keep data and files backed up, protected, synced, and accessible on all our devices. This OneDrive app lets us view and share OneDrive files and documents with all team members.

The ABS' IT department maintains appropriate cybersecurity controls consistent with the U.S. Government Risk Management Framework for cybersecurity and other IT-security requirements. We will be glad to provide additional information on these controls as requested.

During CFD simulations, data will be stored in a dedicated directory on ABS' HPC cluster. In the OpenFOAM style, each case will have a separate case folder. Each case folder will contain different time folders, which store data for the entire flow field at the associated simulation time. The case folder will also contain separate output files, each containing certain flow variables being monitored every time step. Once a simulation is completed, post-processing scripts can be run for further integration or extraction of the raw output data. The resulting data files will also be saved under the main case folder.

For confidentiality, the project data will remain in-house between ABS and HEC. The data from which the graphics, tables, and charts are produced for the final report will be submitted to the MHK-DR, as required.

6.5.2 Data Processing

The following measures will be taken to monitor the data quality in run-time. The CFD software OpenFOAM has the capability of outputting average and maximum Courant number of the entire flow field, which altogether indicate the numerical stability of the simulation. Once the Courant numbers become too high, the simulation could be unstable. Other output files including a general log file and data files for monitoring the total thrust and total torque are updated on the fly every time step. The modeler will inspect data trends frequently, following ABS' CFD best practices, to identify potential problems in the

simulation as early as possible.

6.5.3 Data Analysis

In the CFD model setup, it always includes various monitors of the flow conditions, either based on the raw data or on processed statistics. The following variables will be stored for the entire computational domain for every design examined. They will be stored at selected time instants after the steady state is attained.

- Three-dimensional velocity components
- Pressure
- Variable k as in the $k-\omega$ SST turbulence model
- Variable ω as in the $k-\omega$ SST turbulence model
- Eddy viscosity ν_t as output of turbulence model

The following variables will be stored for every time step throughout the simulation for each design examined:

- Total thrust on the turbine blades and on the hub separately
- Total torque on the turbine blades and on the hub separately

Moreover, the following variables will be calculated and averaged for the steady state:

- Flow rate through a virtual disc 10 cm upstream of the turbine intake plane
- Power coefficient
- Thrust coefficient
- Torque coefficient

Once a simulation is completed, the output time series, including thrust and torque, will be plotted out and inspected. The final steady state will be identified. The turbine performance indicators representing a particular design should always be based on the averages over this steady state. When performing time averaging, we always select full oscillation cycles in order to minimize the error.

After all designs have been examined, the power coefficient of all cases will be demonstrated on the same graph for inspection and comparison.

Although it is well understood that every CFD simulation may have some uncertainty and errors, we will focus on the relative difference and improvement between designs. The uncertainties that are common to all cases will be minimized in the conclusion.

7 PROJECT OUTCOMES

7.1 RESULTS

7.1.1 CFD Model Setup

CFD model setup has been described in Section 6.1. It was assumed that the current turbine was well underneath the free water surface, so the free surface effect would be negligible. Thus, the free water surface was not included in the modeling, which also means that no hydrostatic pressure gradient was considered.

Figure 5 illustrates the computational domain and the boundary conditions. The inlet boundary was set with a uniform flow of 1.5 m/s; the outlet boundary was set as a pressure outlet. The four sides of the domain were free slip walls. Figure 6 shows the perspective view of the computational domain, including the current turbine and three boundaries.

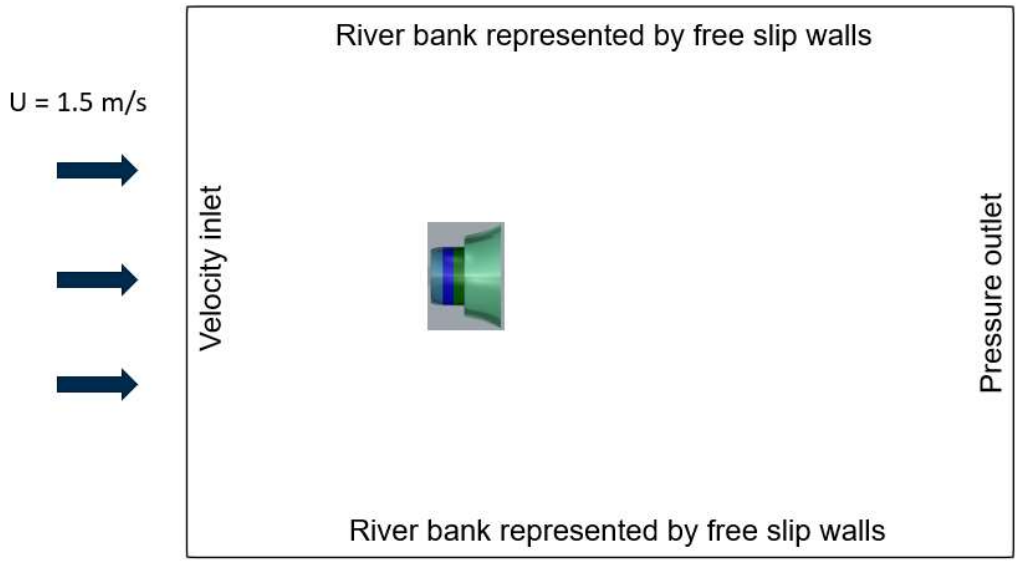

Figure 5. The computational domain with boundary conditions.

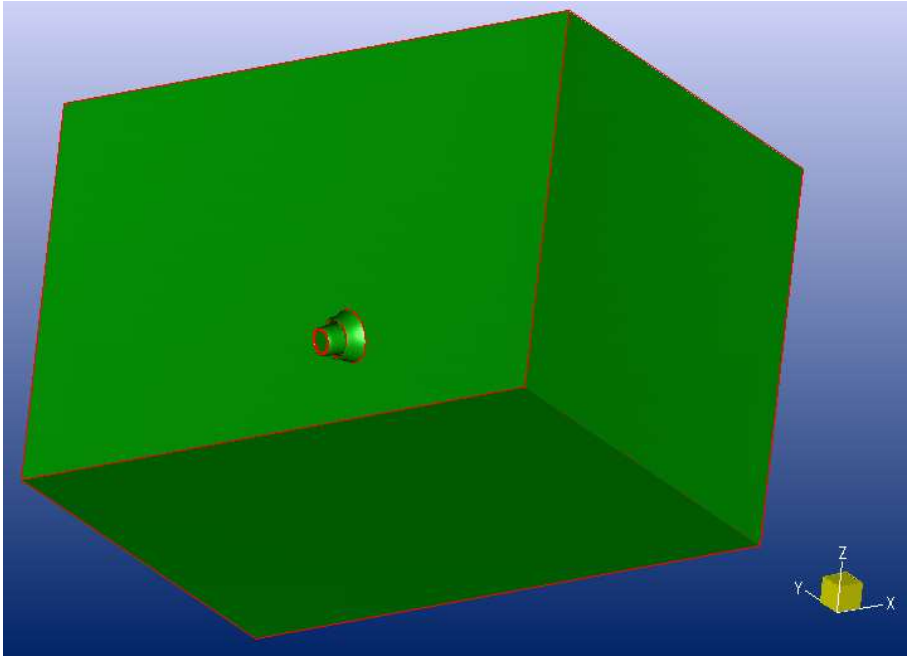

Figure 6. The computational domain with the current turbine and three domain boundaries shown: bottom, side, and outlet.

The AMI (Arbitrary Mesh Interface) method was adopted for handling the rotating grid domain around the rotor. AMI, as implemented in OpenFOAM [1], is particularly efficient for rotor machinery applications, such as turbines and propellers. AMI can save many grid cells and much computational time because there are no overlapping grids which would otherwise require high computational loads for interpolation as for the overset grid method.

Figure 7 shows the rotor grid domain and its surface mesh for the 4-bladed baseline design. Figure 8 presents the assembled volume mesh, consists of the rotor and the stator grids, and its surface mesh of a 3-bladed rotor design. The struts between the shroud and the diffuser were omitted for simplification. For the 3-bladed baseline rotor, the rotor grid had 2.1 million cells, and the baseline stator grid had 4.2 million cells. The time-steps were set to 0.001 s or 0.002 s, depending on the actual rotor Revolutions Per Minute (RPM). It is important to note that the so-called “baseline” design refers to that of HEC version 4.1.8.

Convergence tests for the time-step and grid-size were first performed and summarized in Appendix 11.3. The best combination of time step and grid size will be used for all design variates.

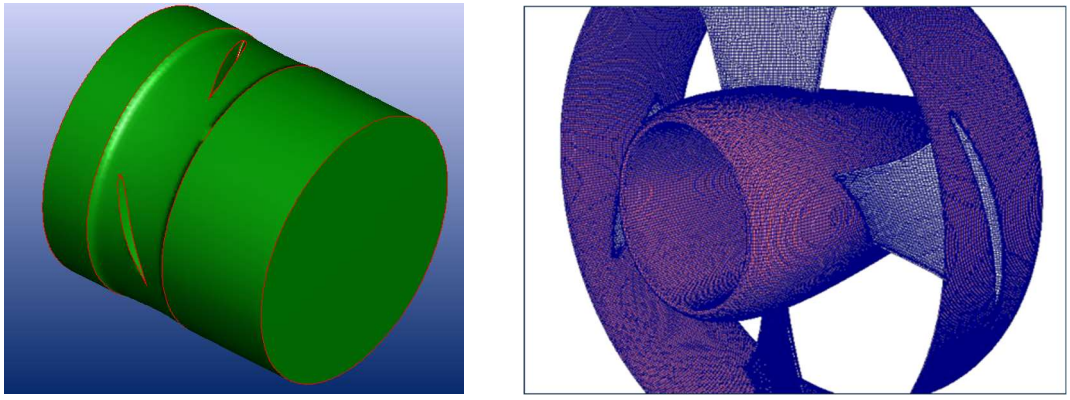

Figure 7. The rotor grid domain (left) and its surface mesh (right) for the 4-bladed baseline design.

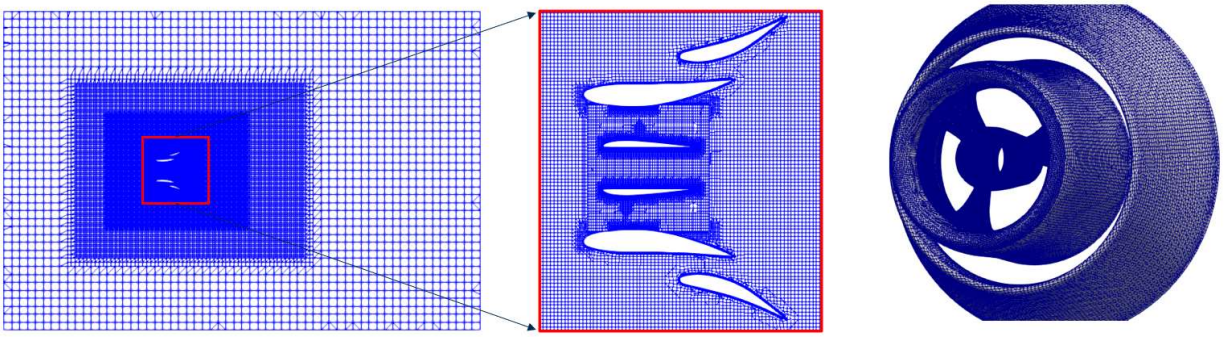

Figure 8. The assembled volume mesh for the entire computational domain as viewed in the plane at y = 0 (left) and a close-up view of the volume and the surface mesh around the turbine (middle and right) for the 3-bladed baseline design.

7.1.2 Geometry Morphing for HEC Water Turbine

An in-house developed "Rhinoscript" using Rhinoceros3D was used to create variates from the baseline design. Since the cross sections of the shroud, the diffuser, and the hub are all similar to a NACA airfoil, the sectional profiles can be characterized by the foil thickness, camber, and the maximum camber location, as shown in Figure 2. By changing these parameters, the script can automatically generate new sectional profiles for the shroud, the diffuser, and the hub, respectively. The development of this script was a critical step in handling such a large number of design variates.

The script was based on Visual Basic (VB) script language embedded in Rhinoceros3D, which could connect with the CAD functionalities of Rhinoceros3D seamlessly. The usage of the script is briefly summarized below:

(1) Extract the edges of the original sectional profile

(2) Join the edges into a full contour of the foil

(3) Enter the values of the thickness, maximum camber, and the maximum camber location at the prompt

(4) Run the script in Rhinoceros3D

(5) A new profile with the specified parameters is created

(6) Revolve the two-dimensional profile into a three-dimensional body (e.g., a shroud, a diffuser, or a hub)

As an example, Figure 9 shows the original sectional profile and the modified profile in different colors for the shroud of the current turbine. Figure 10 presents the three-dimensional shroud surface generated by revolving the obtained foil profile.

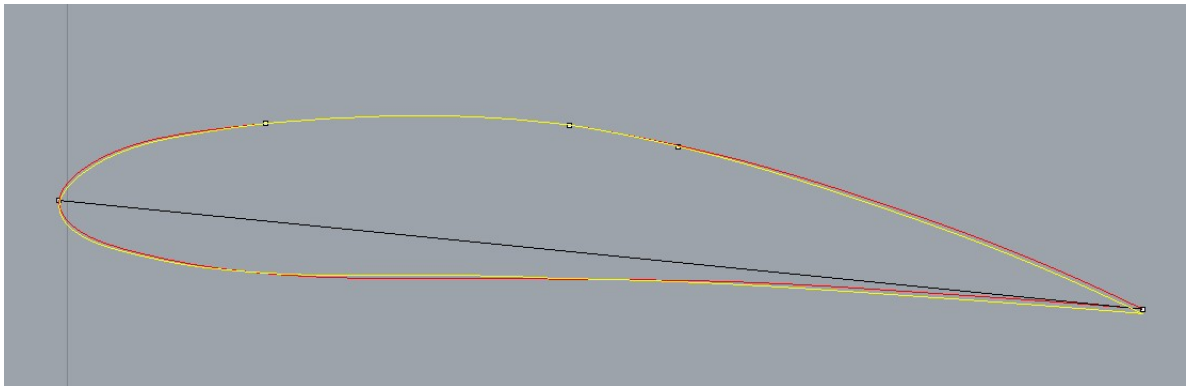

Figure 9. The original and the morphed foil profiles for the shroud of the current turbine (red: the original profile of the baseline design; yellow: the morphed profile as a design variate).

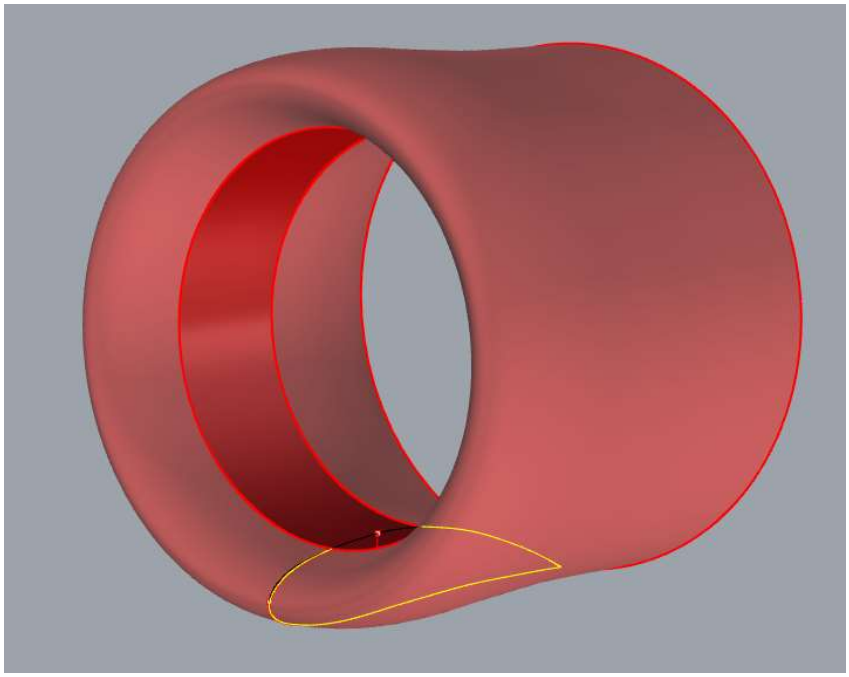

Figure 10. The shroud surface generated by revolving the morphed foil profile (the yellow curve).

It should be noted that for the diffuser there would also be variation of the diameter and the expansion angle, which was done manually.

7.1.3 Study of Baseline Design

It was understood that the first step of the study would be to determine the best number of rotor blades. To this end, the baseline design with different numbers of blades (i.e., 3, 4, and 5) was evaluated using CFD. We followed the common practice, where the rotor will assume a series of constant RPM [2]. Once the simulation attains a steady state, the resulting thrust and torque values as well as the power and torque coefficients can be obtained. In the present study, we tested eight RPMs, from 50 to 400, with an interval of 50 RPM.

Figure 11 shows the pattern of the velocity component Ux (i.e., in the streamwise direction) in the plane of y = 0 (i.e., the center plane) for the 3-bladed configuration at 200 RPM. Figure 12 shows the dynamic pressure distribution at the center plane for the same case. Figure 13 presents the upstream/downstream views of the dynamic pressure distributions on the surfaces of the 3-bladed baseline turbine. Figure 14 shows the convergence history of the thrust and the torque, respectively, for the same 3-bladed baseline design at 200 RPM.

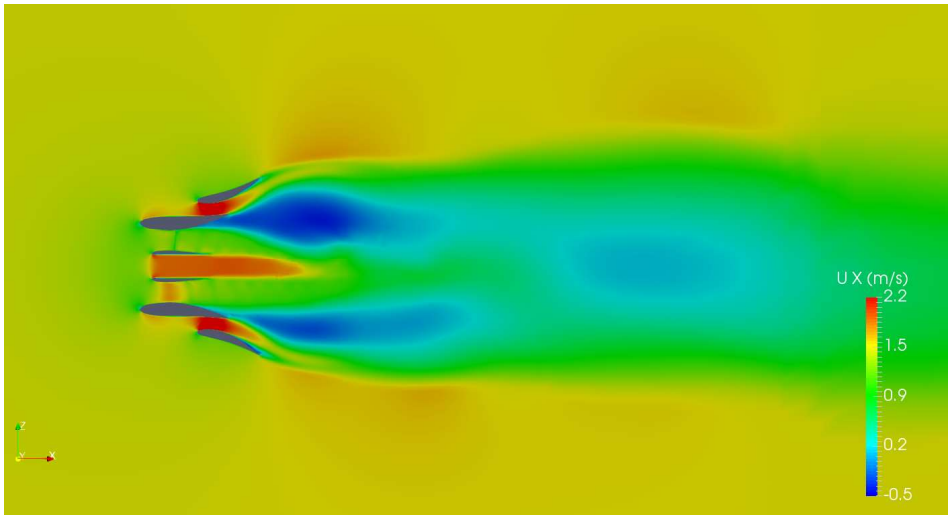

Figure 11. CFD-simulated velocity component Ux at y = 0 (RPM 200, baseline design, 3-bladed).

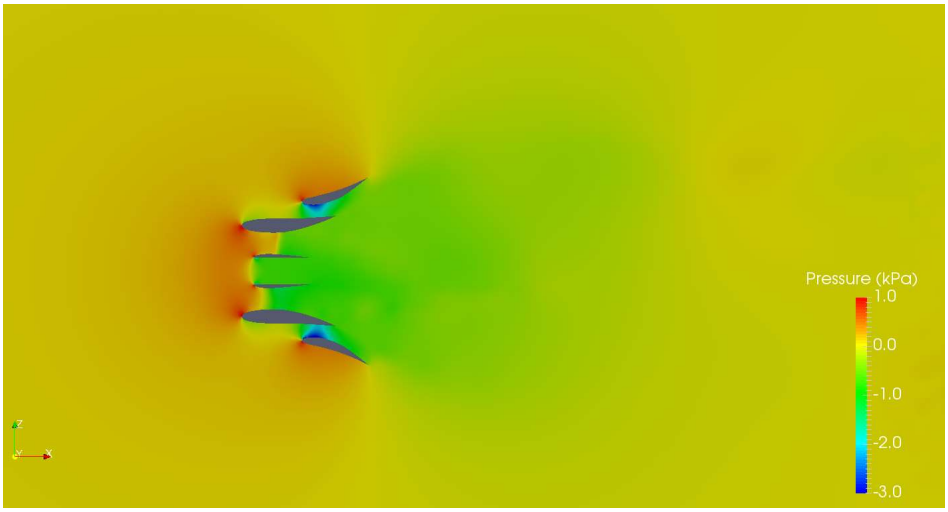

Figure 12. CFD-simulated distribution of dynamic pressure at y = 0 (RPM 200, baseline design, 3-bladed).

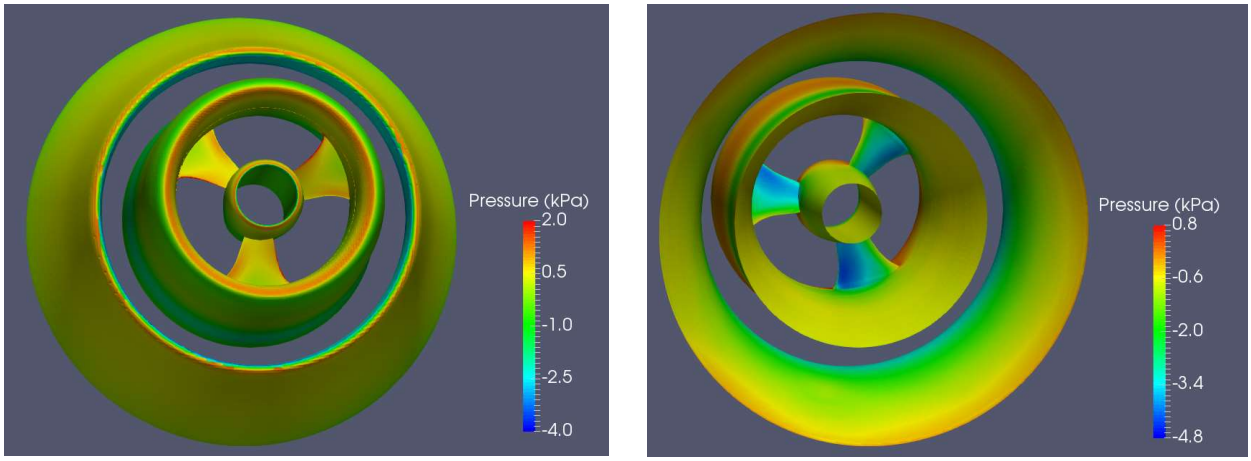

Figure 13. CFD-simulated dynamic pressure on the turbine body (left: viewed from upstream; right: viewed from downstream. RPM 200, Baseline design, 3-bladed)

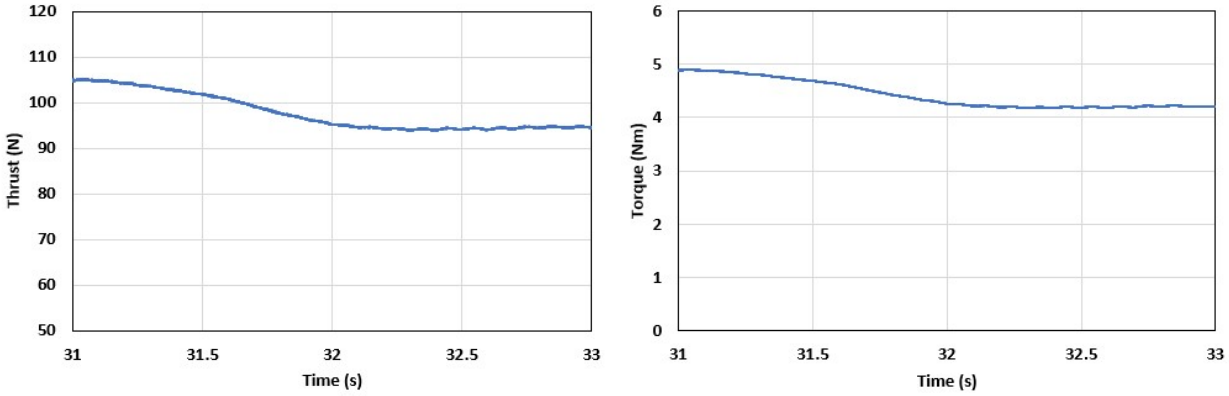

Figure 14. Convergence histories of the thrust (left) and the torque (right) of the rotor (RPM 200, baseline design, 3-bladed).

Figure 15 shows a comparison of the torque and power for the baseline design with different number of blades at different RPMs.

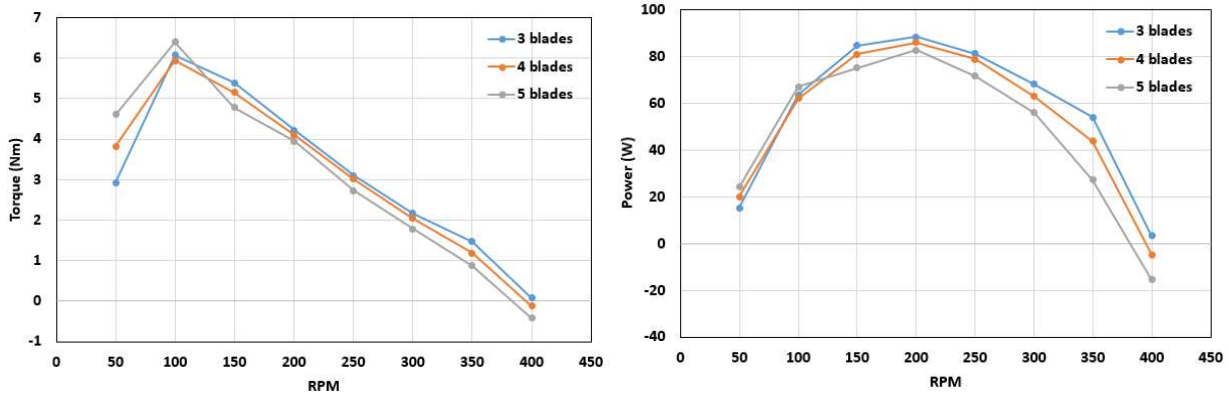

Figure 15. The torque curves (left) and power curves (right) for the baseline design with different numbers of blades.

Apparently, the baseline designs with different numbers of blades all attained their respective maximum power outputs at 200 RPM. Of them, the 3-bladed baseline design appears to deliver the highest power. Detailed data are shown in Table 2 for the 3-bladed design.

Table 2. The steady state torque and power at various RPMs (baseline design, 3-bladed).

RPM	Torque (Nm)	Power (W)
50	2.92	15.29
100	6.07	63.56
150	5.39	84.67
200	4.22	88.38
250	3.1	81.16
300	2.17	68.17
350	1.47	53.88
400	0.076	3.2

The curves of the torque coefficient, C_Q, and the power coefficient, C_P, are shown in Figure 16, based on the definitions below:

$$C_Q = \frac{Q}{\frac{1}{2}\rho A\ ^2 R} \tag{1}$$

$$C_P = \frac{\Omega Q}{\frac{1}{2}\rho A V^3} \tag{2}$$

where Q denotes the torque, Ω is the angular speed, ρ is the water density, V is the inflow velocity, R is the turbine radius, and $A = \pi R^2$ is the rotor swept area. The Tip Speed Ratio (TSR) is defined as:

$$TSR = \frac{\Omega R}{V} \tag{3}$$

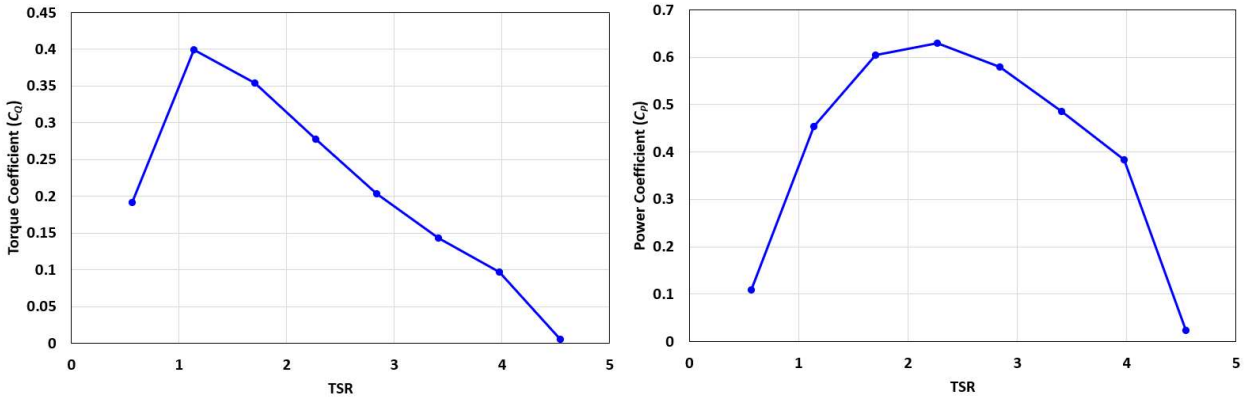

Figure 16. Torque coefficient (left) and power coefficient (right) versus the TSR for the baseline design (3-bladed).

For design variates, we only conducted CFD simulation for the RPM of 200, rather than for the entire range of RPMs. We assume that with minor local changes in the geometry the RPM for the highest power output will not be altered. We also will only focus on 3-bladed design variates following the same reasoning.

Starting with the optimal baseline design (i.e., with three blades), the parametric study was conducted in three stages in order: modifications of the shroud geometry, the diffuser geometry, and the hub geometry. Upon completion of each stage, an intermediate optimal design is identified. For example, the optimal design after modifying the diffuser geometry implies that the shroud geometry modification has also been done.

7.1.4 Study of Shroud Variates

To evaluate different shroud variates, the key parameters for the shroud were varied (as described in Figure 2) and CFD was conducted for each variate as below:

- Changing the maximum camber by ±10% (3 levels)
- Changing the thickness by +10% (2 levels)
- Changing the maximum camber location by ±10% (3 levels)

The case setup and gridding were all based on the setup for the converged case for the baseline design (3 blades) with the maximum power output (Section 7.1.1). The stator grid was re-generated by only swapping out the shroud geometry. The boundary/initial conditions were not changed in the CFD simulations. The RPM was kept at 200 targeting the maximum power output.

For the ease of presentation, we show results in two groups: "Thickness 1.0", i.e., the original thickness (Table 3) and "Thickness 1.1", i.e., with a thickness increased by +10% (Table 4). A reduced thickness, on the other hand, was not intended from the design point of view. For either thickness value, we arrange results for different levels of the maximum camber value and its location.

Table 3. The attained steady-state power output (unit: W) for Group Thickness 1.0 for the shroud (RPM 200). The case highlighted in yellow is the optimal baseline design (i.e., 3-bladed and at 200 RPM) from the previous step. The case highlighted in green is the one with the highest power output among all different shroud variates as in both Tables 3 and 4.

Max. camber location\Max. camber	0.9	1.0	1.1
0.9	84.31	86.62	87.06
1.0	86.39	88.38	84.63
1.1	89.49	88.49	84.41

Table 4. The attained steady-state power output (unit: W) for Group Thickness 1.1 for the shroud (RPM 200).

Max. camber location\Max. camber	0.9	1.0	1.1
0.9	87.02	84.86	85.51
1.0	87.61	87.52	86.39
1.1	83.34	84.30	87.34

In Figure 17, the power outputs of all cases in the two shroud thickness groups are compared along with that of the 3-bladed baseline design. The optimal design after modifying the shroud is the one with the maximum camber decreased by 10%, the maximum camber location increased by 10%, and the thickness unchanged. Therefore, a thinner and flatter sectional shape of the shroud will tend to result in a higher power output. However, modifying the shroud alone only increased the power output by 1.3% compared to the 3-bladed baseline design.

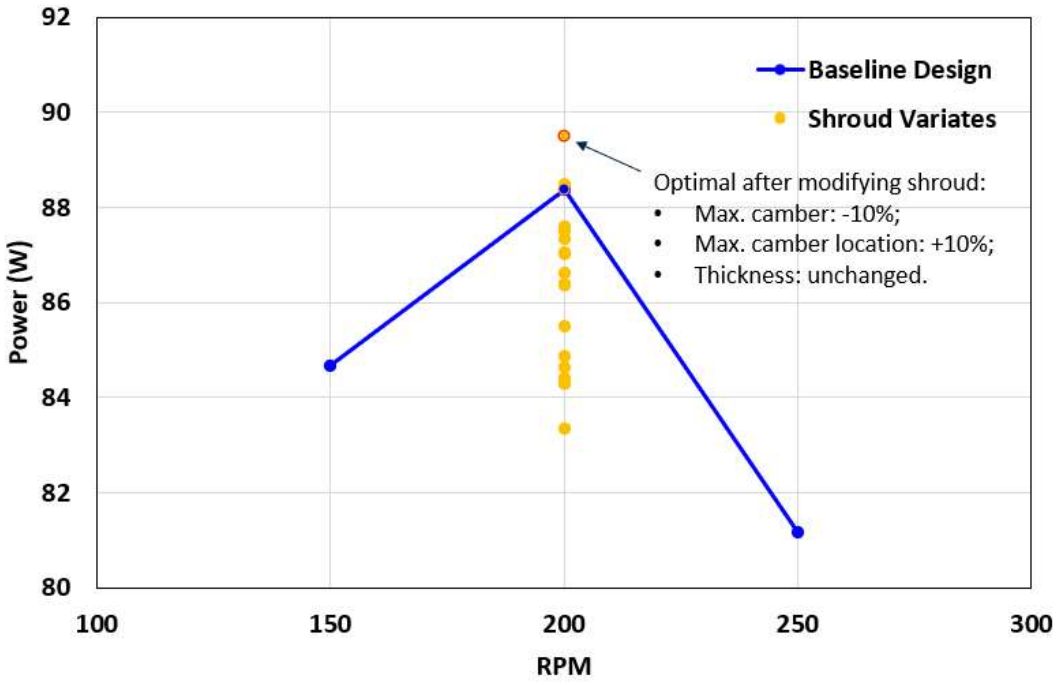

Figure 17. Output power for all cases with morphed shroud geometries compared with that of the 3-bladed baseline design (RPM 200).

Figure 18 shows the pattern of the velocity component Ux at the plane of y = 0 for the optimal design after modifying the shroud geometry. Figure 19 shows the dynamic pressure distribution at the plane of y = 0 for the same case. Figure 20 presents the upstream/downstream views of the dynamic pressure distributions on the surfaces of the 3-bladed current turbine for the optimum design after modifying the shroud geometry.

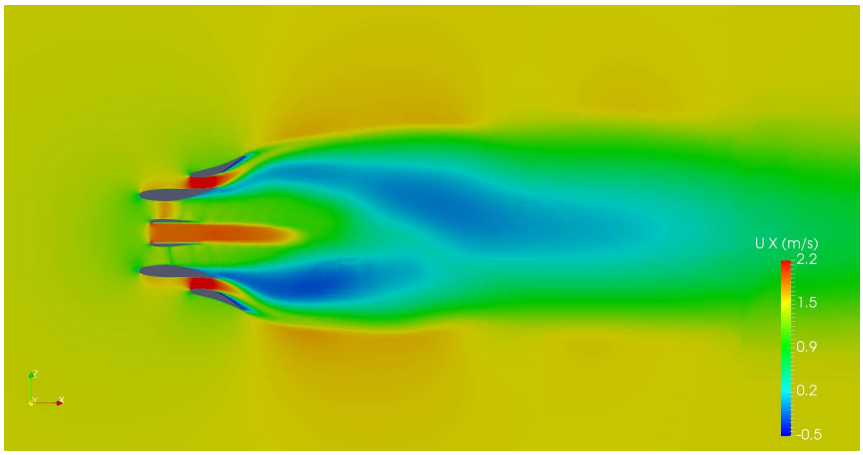

Figure 18. CFD-simulated velocity component Ux at y = 0 for the optimal design after modifying the shroud geometry (RPM 200, 3-bladed).

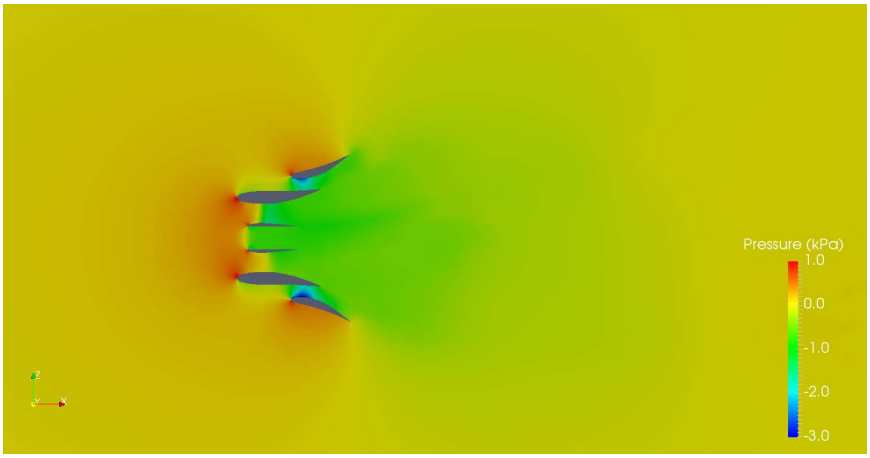

Figure 19. CFD-simulated dynamic pressure pattern at y = 0 for the optimal design after modifying the shroud geometry (RPM 200, 3-bladed).

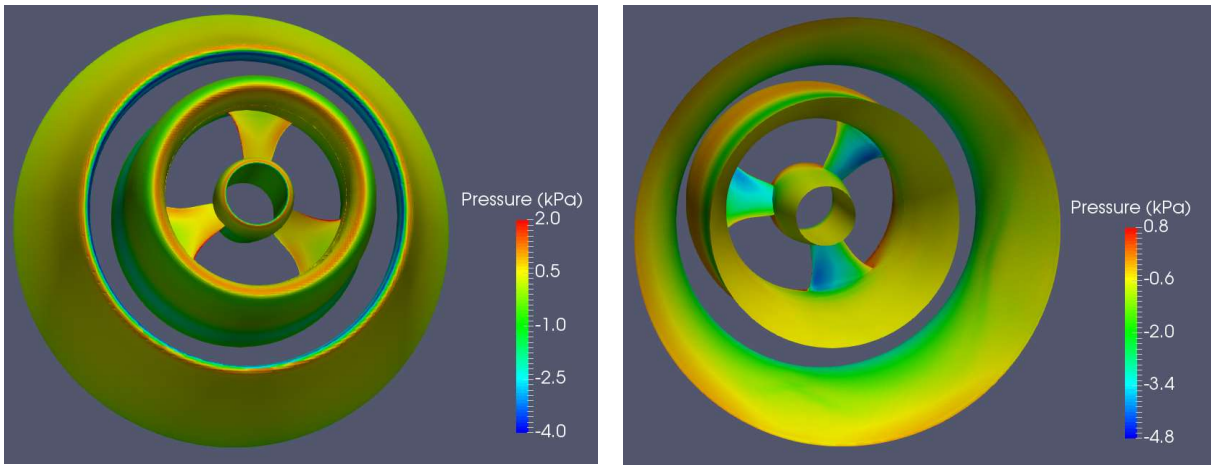

Figure 20. CFD-simulated dynamic pressure distribution on the turbine surfaces for the optimal design after modifying the shroud geometry (left: viewed from upstream; right: viewed from downstream; RPM 200, 3-bladed).

7.1.5 Study of Diffuser Variates

The next step was to modify the diffuser geometry starting from the optimal design as identified from the previous step (Section 7.1.4). The key parameters to change for the diffuser are given as follows.

- Changing the maximum camber by ±10% (3 levels)
- Changing the thickness by ±10% (3 levels)
- Changing the maximum camber location by ±10% (3 levels)
- Increasing the diffuser diameter by +10% (2 levels)
- Increasing the diffuser expansion angle by +4 degrees (2 levels)

As for the shroud cases, the gridding for the different diffuser cases will only affect the local meshes around the diffuser. The boundary/initial conditions were not changed in the CFD simulations, and the RPM was kept at 200 targeting the maximum power output.

For the ease of presentation, we assign the cases into four groups, i.e., “E1D1”, “E1D2”, “E2D1”, and “E2D2” (108 cases in total). Here, “E” means expansion; “D” means diameter; the number “1” or “2” means different value levels. Since we have two expansions angles, “E1” means the original expansion angle and “E2” means the increased level (+4 degrees). Similarly, “D1” means the original diameter, while “D2” means the increased level, i.e., +10% of the original.

Table 5 shows the CFD-simulated steady-state torque values for the diffuser variates in the E1D1 group. Results for different cases are arranged in three two-way tables with different thickness, maximum camber, and maximum camber location levels. From Table 5, two trends were observed:

- Increased maximum camber (from 1 to 1.1) will lead to decreased torque, and hence lower power output
- Increased thickness (from 1 to 1.1) will lead to decreased torque, and hence lower power output

These observations are consistent with those from the shroud cases. In order to reduce computational time, ABS and HEC both agreed to only evaluate the cases with changed parameters that were anticipated to increase power output for the three remaining groups. This approach could be seen as a proactive search strategy, as opposed to running through a pre-defined case matrix blindly. Some cases, with unfavorable diffuser parameters, were still evaluated using CFD as verification of this new search strategy. The results for the three remaining groups are shown in Tables 6, 7, and 8, respectively. Clearly, none of the verification cases produced a higher torque than the one highlighted in Table 8 identified by the search strategy.

Table 5. Steady-state torque values for different diffuser variates (Group E1D1, unit: Nm); the case highlighted in yellow is for the optimal design up to the previous step (i.e., after modifying the shroud geometry).

Thickness 0.9

Max. camber location\Max. camber	0.9	1.0	1.1
0.9	4.48	4.42	4.40
1.0	4.28	4.47	4.41
1.1	4.44	4.45	4.30

Thickness 1.0

Max. camber location\Max. camber	0.9	1.0	1.1
0.9	4.45	4.47	4.26
1.0	4.48	4.27	4.24
1.1	4.51	4.34	4.23

Thickness 1.1

Max. camber location\Max. camber	0.9	1.0	1.1
0.9	4.40	4.32	4.17
1.0	4.23	4.25	4.22
1.1	4.31	4.29	4.20

Table 6. Steady-state torque values for different diffuser variates (Group E1D2, unit: Nm); the cases associated with the blank cells were skipped; the cases with torques in red were skipped first and then selected for a full CFD evaluation as a verification of the search strategy.

Thickness 0.9

Max. camber location\Max. camber	0.9	1.0	1.1
0.9	4.42	4.50	4.22
1.0	4.49	4.36	
1.1	4.34	4.52	

Thickness 1.0

Max. camber location\Max. camber	0.9	1.0	1.1
0.9	4.35	4.45	
1.0	4.42	4.43	
1.1	4.43	4.45	4.32

Thickness 1.1

Max. camber location\Max. camber	0.9	1.0	1.1
0.9	4.27		
1.0			
1.1			

Table 7. Steady-state torque values for different diffuser variates (Group E2D1, unit: Nm); the cases associated with the blank cells were skipped; the cases with torques in red were skipped first and then selected for a full CFD evaluation as a verification of the search strategy.

Thickness 0.9

Max. camber location\Max. camber	0.9	1.0	1.1
0.9	4.39	4.44	4.28
1.0	4.29	4.44	
1.1	4.41	4.48	4.31

Thickness 1.0

Max. camber location\Max. camber	0.9	1.0	1.1
0.9	4.40	4.39	
1.0	4.42	4.60	4.25
1.1	4.38	4.39	

Thickness 1.1

Max. camber location\Max. camber	0.9	1.0	1.1
0.9	4.32		
1.0			
1.1			

Table 8. Steady-state torque values for different diffuser variates (Group E2D2, unit: Nm); the cases associated with the blank cells were skipped; the cases with torques in red were skipped first and then selected for a full CFD evaluation as a verification of the search strategy. The case highlighted in green is the optimal design after modifying the diffuser geometry.

Thickness 0.9

Max. camber location\Max. camber	0.9	1.0	1.1
0.9	4.69	4.68	
1.0	4.74	4.70	4.59
1.1	4.77	4.69	4.67

Thickness 1.0

Max. camber location\Max. camber	0.9	1.0	1.1
0.9	4.70	4.66	4.57
1.0	4.67	4.72	4.64
1.1	4.72	4.66	

Thickness 1.1

Max. camber location\Max. camber	0.9	1.0	1.1
0.9	4.62	4.54	
1.0	4.61		4.51
1.1			

Figure 21 shows the torque values for all diffuser cases together. The optimum design so far has the expansion angle increased by 4 degrees, the diameter increased by 10%, the thickness decreased by 10%, the maximum camber decreased by 10%, and the maximum camber location increased (i.e., moved downstream) by 10%. These directions of the changes in the parameters indicate that lower obstruction of the turbine structures to the incident current flow (e.g., larger expansion, larger diameter, smaller thickness, and flatter sectional profile) will help increase torque (and power). This is consistent with all previous observations. The diffuser geometry appears to have the largest influence on the output power (or torque). The power has increased 13% from the previous optimal design (i.e., after modifying the shroud geometry) to the current optimal design.

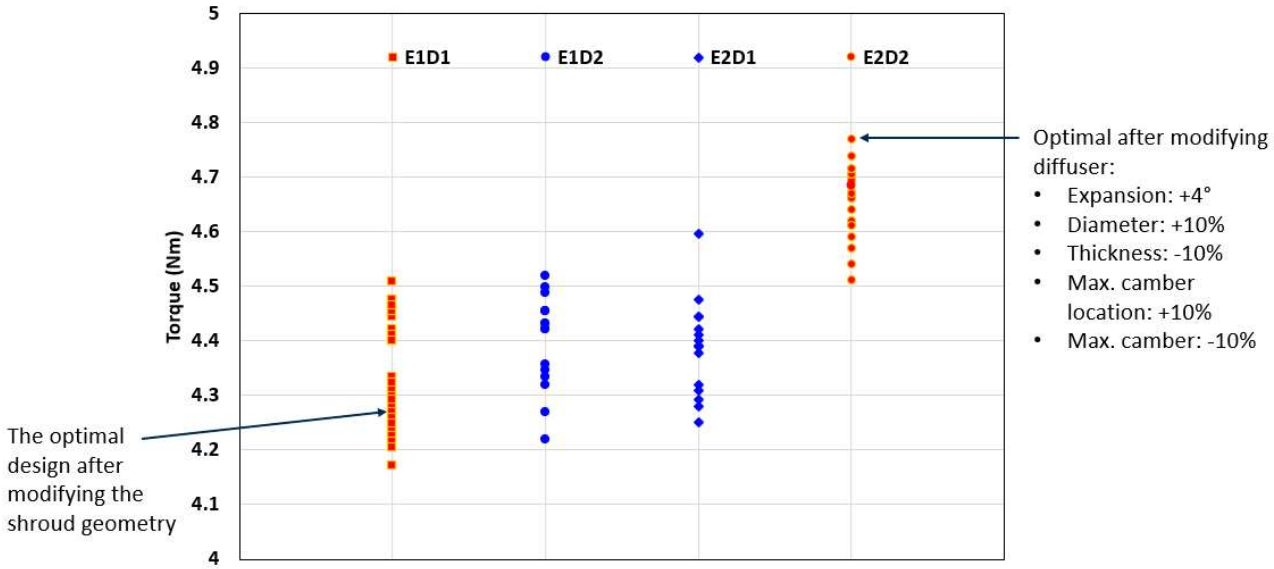

Figure 21. Torque values for all diffuser cases (RPM 200)

Figure 22 shows the pattern of the velocity component Ux in the plane at y = 0 for the optimal design up to this point. Figure 23 shows the dynamic pressure distribution in the plane of y = 0 for the same design. Figure 24 presents the upstream/downstream views of the dynamic pressure distributions on the surfaces of the same design.

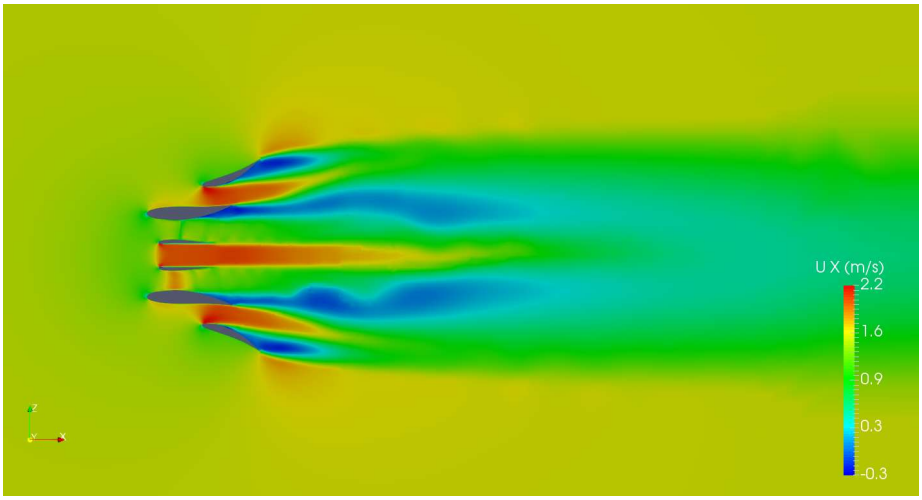

Figure 22. CFD-simulated velocity component Ux at y = 0 for the optimal design after modifying the diffuser geometry (RPM 200, 3-bladed).

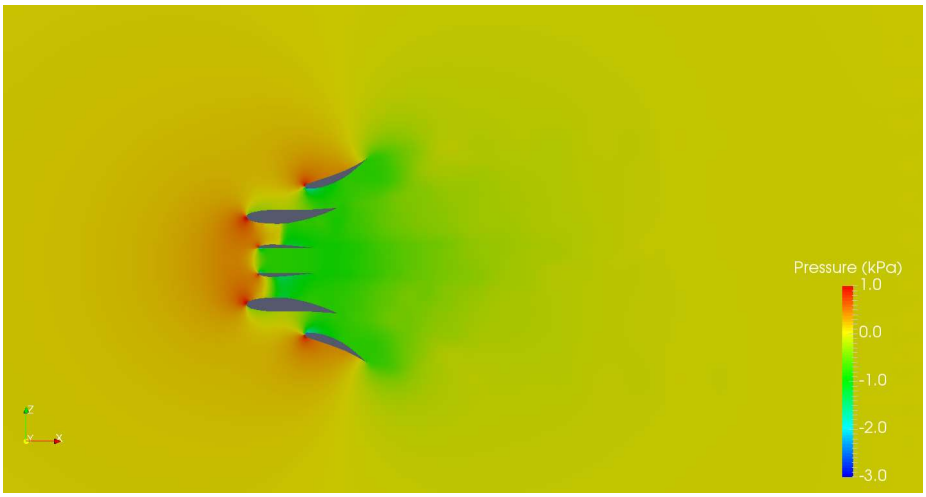

Figure 23. CFD-simulated dynamic pressure at y = 0 for the optimal design after modifying the diffuser geometry (RPM 200, 3-bladed)

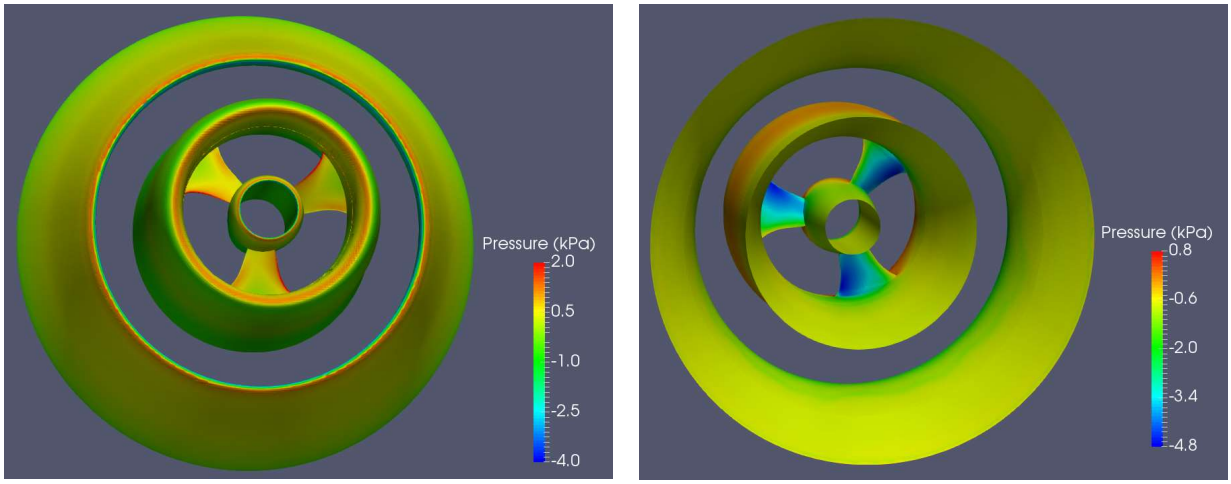

Figure 24. CFD-simulated dynamic pressure on the turbine surfaces for the optimal design after modifying the diffuser geometry (left: viewed from upstream; right: viewed from downstream. RPM 200; 3-bladed).

7.1.6 Study of Hub Variates

To evaluate different hub geometries, we perturbed a set of sectional parameters as for the shroud and for the diffuser:

- Changing the maximum camber by ±10% (3 levels)
- Changing the thickness by ±10% (3 levels)

In order to maintain the highest comparability across cases, the computational grids for any new case will only differ around the local geometrical changes. The boundary/initial conditions were not changed in the CFD simulations. The rotor RPM was kept at 200 targeting the maximum power output. The attained steady-state torques for all hub cases are listed in Table 9. It is easy to identify that the optimal design after modifying the hub geometry had both maximum camber and thickness reduced by 10% from the original values, respectively. Since all three bodies, i.e., the shroud, the diffuser, and the hub, have been modified, this optimal design in Table 9 is also the *final optimal design* from the entire parametric study.

Table 9. Steady-state torque values for different hub variates (unit: Nm). The case highlighted in yellow is the previous optimal design after modifying the diffuser geometry; the case highlighted in green is the current optimal design after modifying the hub geometry.

Max. camber\Thickness	0.9	1.0	1.1
0.9	4.86	4.82	4.76
1.0	4.81	4.77	4.73
1.1	4.81	4.74	4.75

The torque values for all hub variates are shown together in Figure 25, along with those for the baseline design (3-bladed). The optimal hub geometry has a thickness decreased by 10% from the original and a maximum camber decreased by 10% from the original. Again, the direction of improvement for the hub is consistent with those for the shroud and the diffuser.

Overall, the maximum power output of the final optimal design (after modifying the hub geometry) realized a 15% increase from that of the baseline design. Considering the simplicity of this parametric study, such an improvement in energy output is incredible.

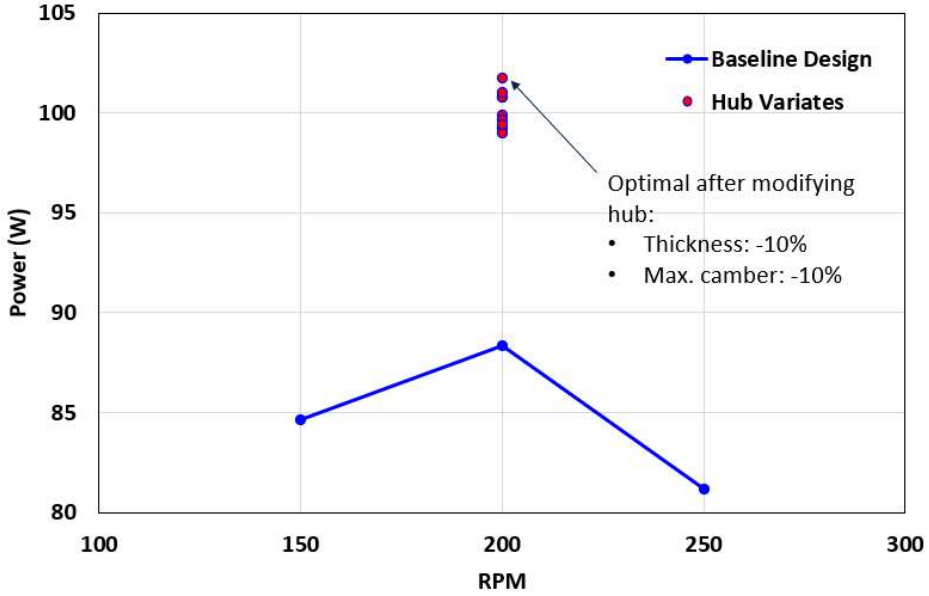

Figure 25. Power output of the baseline turbine and the variates with different hub geometries (RPM 200).

Figures 26 and 27 show the patterns of the velocity component Ux in the plane at y = 0 as viewed from upstream and downstream, respectively. Figure 28 shows the dynamic pressure distribution in the plane at y = 0. Figure 29 presents the upstream/downstream views of the dynamic pressure distributions on the surfaces of the current optimal design.

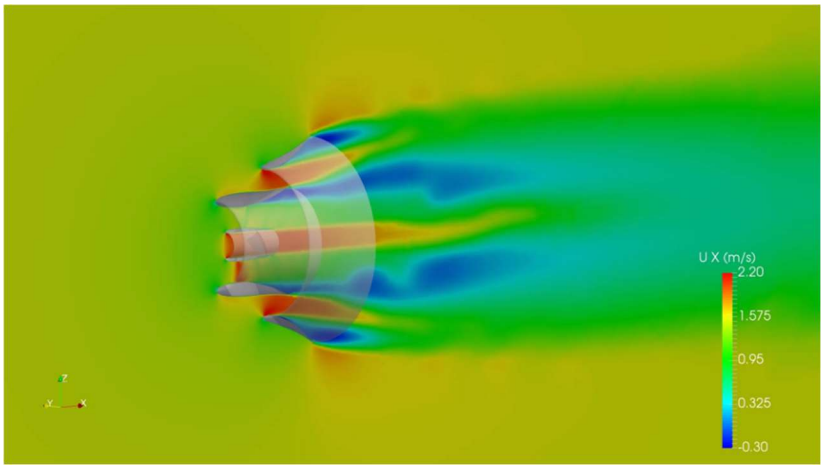

Figure 26. CFD-simulated velocity component Ux viewed from upstream in the plane at y = 0 for the optimal design (RPM 200, 3-bladed).

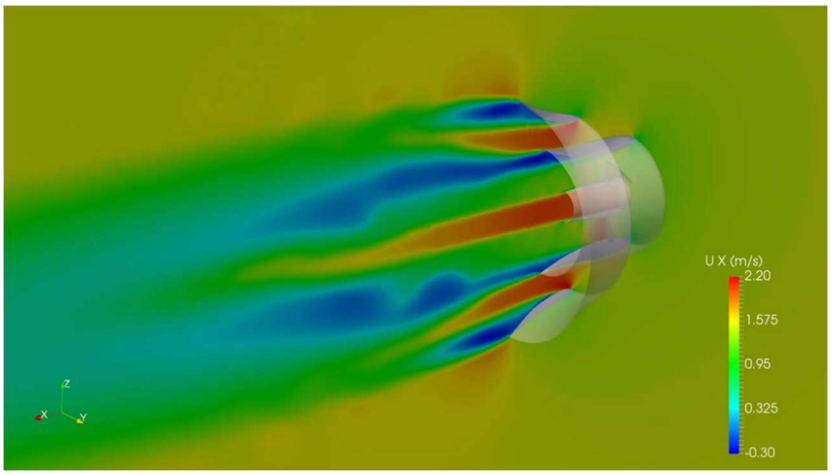

Figure 27. CFD-simulated velocity component Ux viewed from downstream in the plane at y = 0 for the optimal design (RPM 200, 3-bladed).

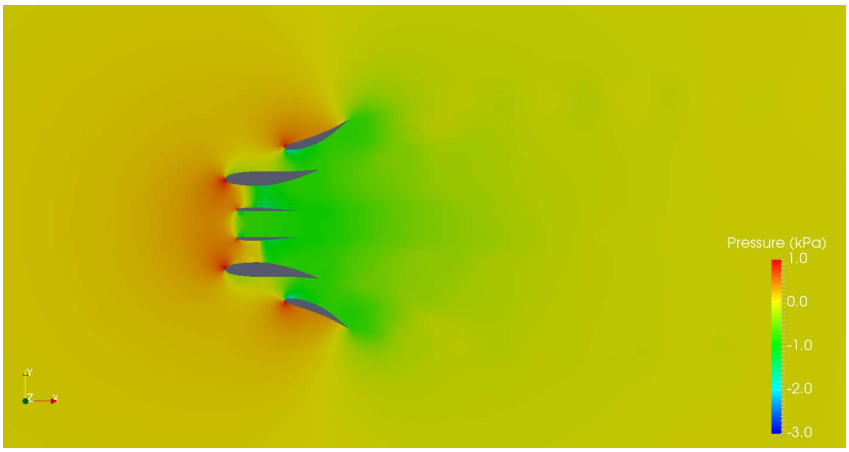

Figure 28. CFD-simulated dynamic pressure in the plane at y = 0 for the optimal design (RPM 200, 3-bladed).

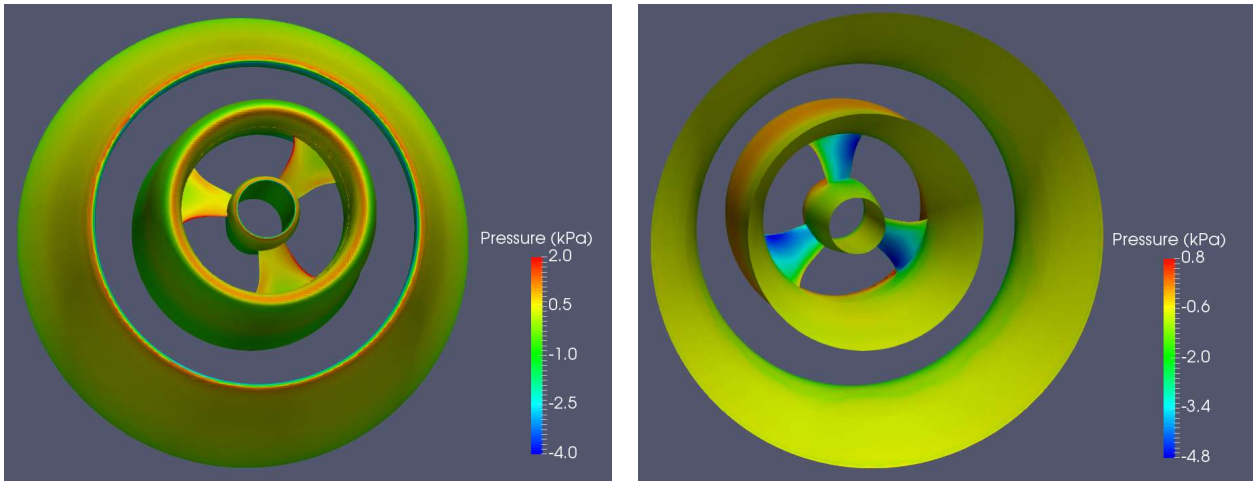

Figure 29. CFD-simulated dynamic pressure on the surfaces of the optimal design (left: viewed from upstream; right: viewed from downstream. RPM 200, 3-bladed).

7.1.7 Hydrodynamic Performance of the Current Turbine

In this section, the hydrodynamic performance of the current turbine is evaluated based on the key performance indicators as follows:

- The torque and power
- The volumetric flow rate through the rotor plane.

Power and Torque

The hydrodynamic performance of the optimal design as identified in Section 7.1.6 for RPMs other than 200 was calculated using CFD. The results are shown in Table 10. It can be confirmed that the maximum power output did occur at 200 RPM, as expected. Figure 30 shows the corresponding torque and power curves, respectively. Figure 31 presents the nondimensional torque coefficient and power coefficient as defined by Equations (1) and (2), respectively. Figure 32 shows the comparison of the optimal designs from different stages.

Table 10. The steady-state torque and power for the final optimal design (3-bladed).

RPM	Torque (Nm)	Power (W)
50	3.22	16.86
100	6.36	66.6
150	5.92	92.99
200	4.86	101.73
250	3.58	93.73
300	2.68	84.19
350	1.64	60.11
400	0.59	24.71

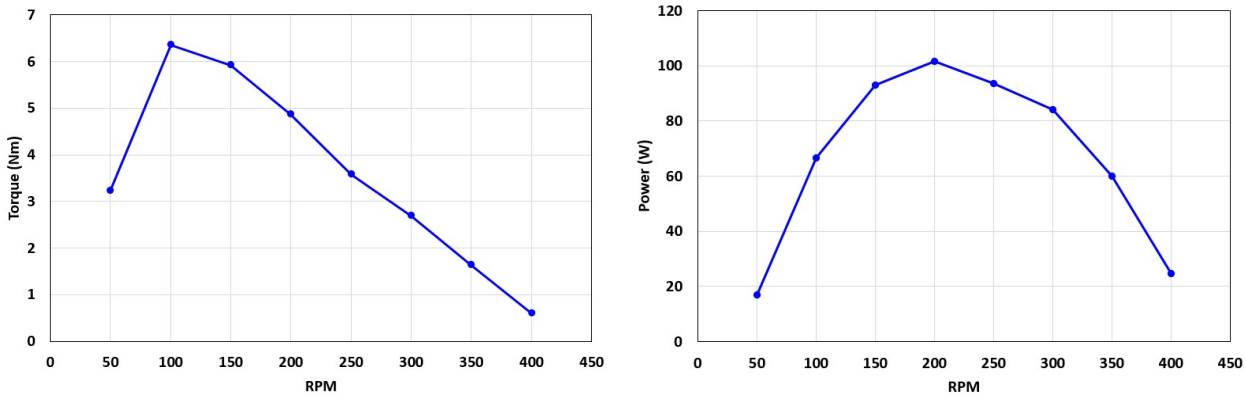

Figure 30. Torque (left) and power (right) versus the rotor RPM for the final optimal design.

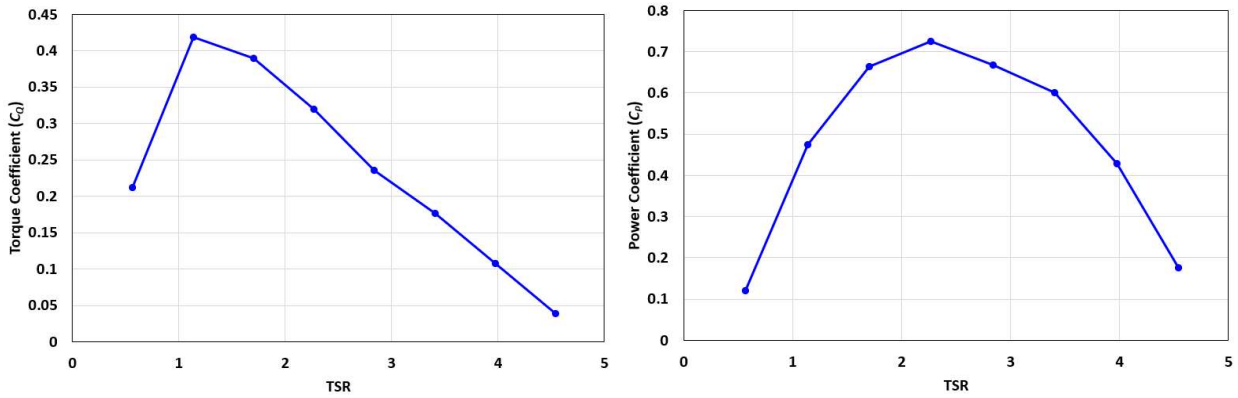

Figure 31. Torque coefficient (left) and power coefficient (right) versus the rotor RPM for the final optimal design.

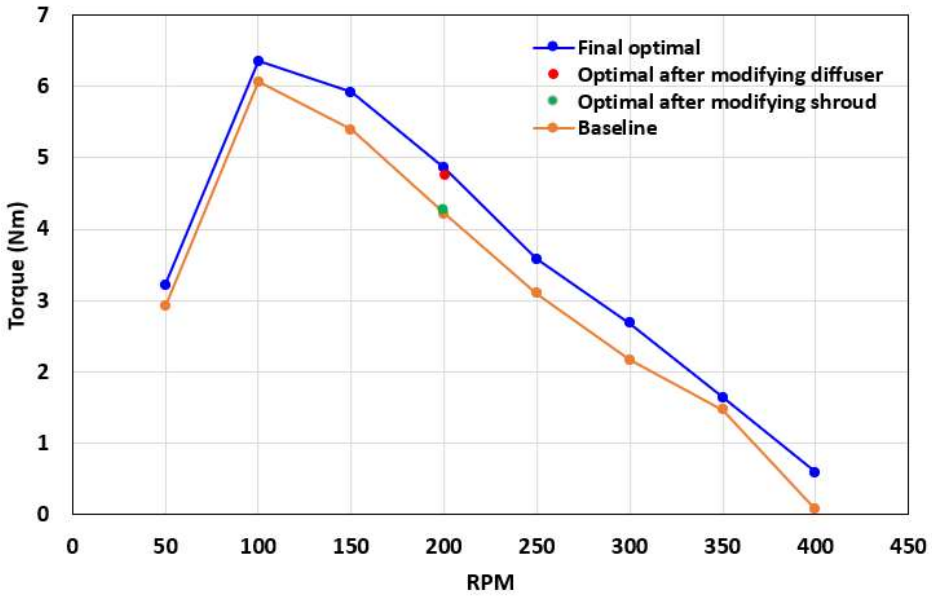

(a)

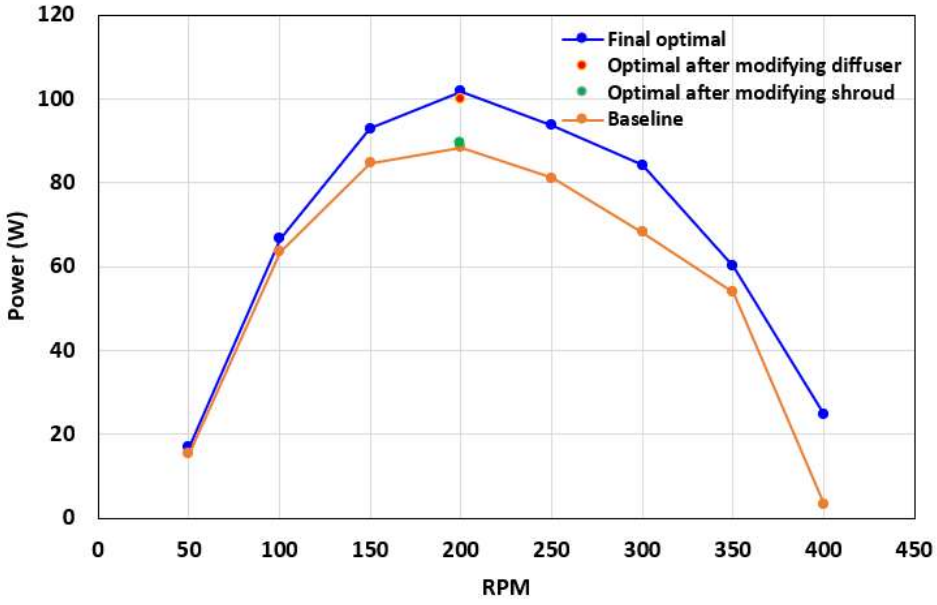

(b)

Figure 32. Comparison of hydrodynamic performance of designs for different stages: (a) torque; (b) power.

Volumetric Flow Rate

The volumetric flow rate through the current turbine was calculated by integrating the local velocities on a virtual disc in front of the rotor and averaging the integral over the steady state. The virtual disc is located 10 cm upstream of the rotor plane, as shown in Figure 33. The volumetric flow rates for the optimal designs from each of the four stages are summarized in Table 11 and shown graphically in Figure 34. Evidently, the volumetric flow rate increased from stage to stage in order.

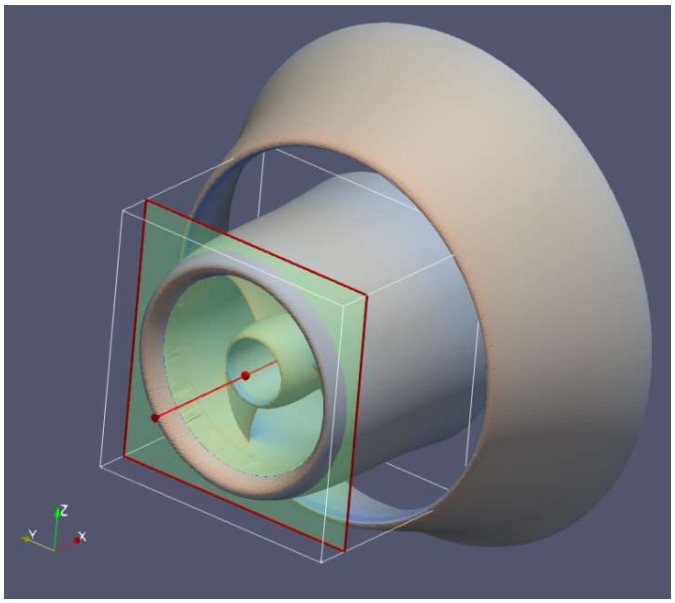

Figure 33. The virtual disc (the green circle inside the shroud located 10 cm upstream of the rotor plane) for calculating the volumetric flow rate through the current turbine.

Table 11. The volumetric flow rate through the optimal turbine from different stages (RPM 200).

Stage	Flow Rate (m^3/s)
Baseline	0.1071
Optimal after modifying shroud	0.1086
Optimal after modifying diffuser	0.1119
Optimal after modifying hub (the final optimal)	0.1129

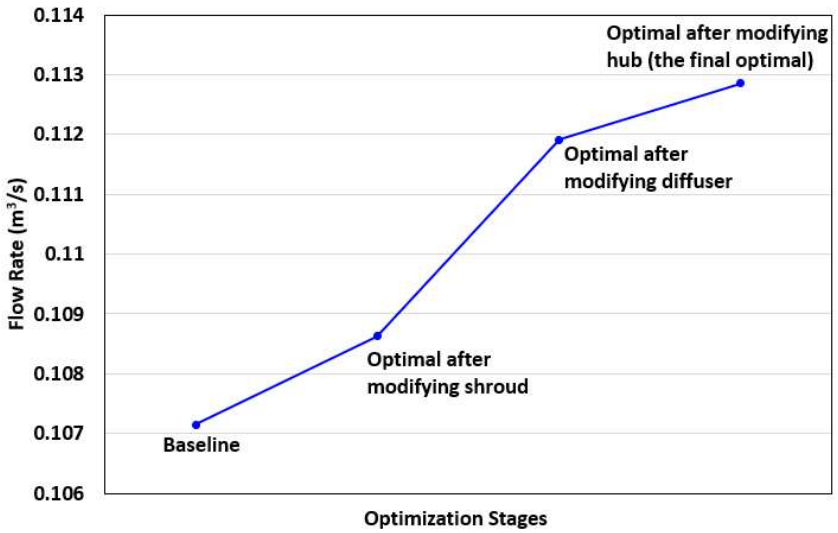

Figure 34. Volumetric flow rates through the optimal designs from different stages (RPM 200).

Figure 35 presents the distributions of the velocity component Ux over the virtual discs for the four optimal designs from their respective stages. It is also clear graphically that the maximum Ux increases from stage to stage in order, which is consistent with the trend as shown in Figure 34.

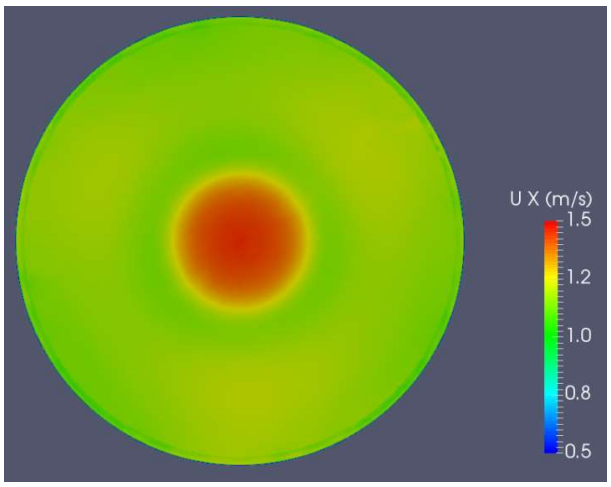

Baseline Design

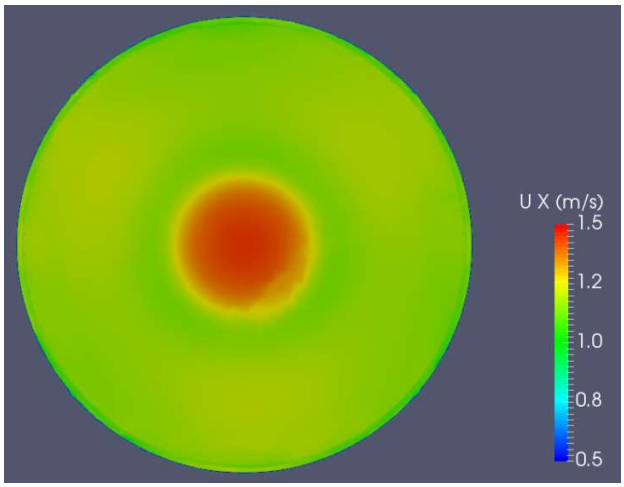

Optimal after modifying shroud

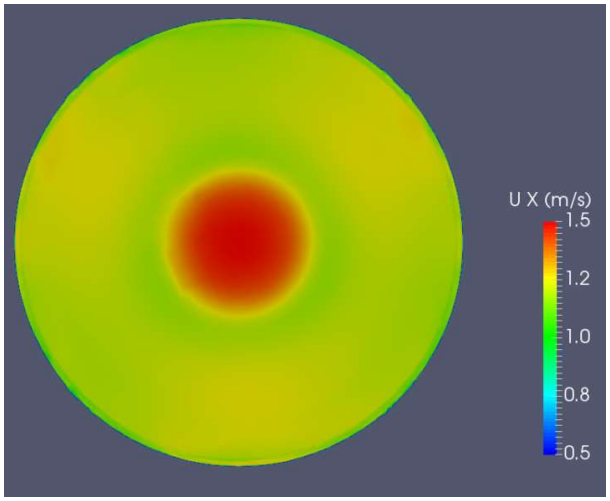

Optimal after modifying diffuser

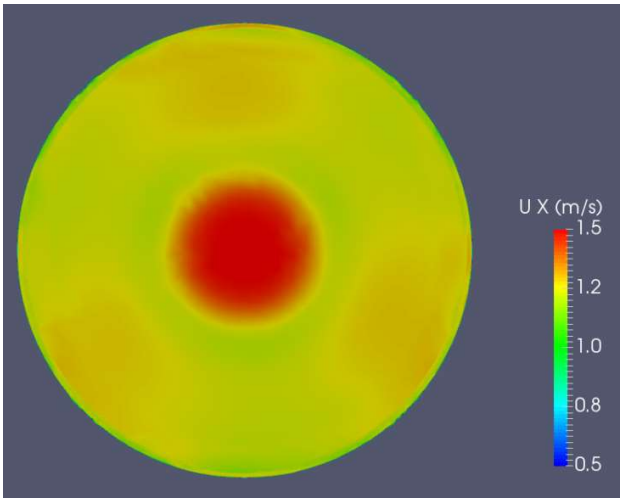

Optimal after modifying hub

Figure 35. CFD-simulated velocity component Ux over the virtual disc 10 cm upstream of the turbine rotor plane for the four optimal designs from different stages (RPM 200).

For the final optimal design, the volumetric flow rates for different RPMs are summarized in Table 12 and shown graphically in Figure 36. It can be observed that the flow rate increases with the increasing RPM monotonically. The flow rate grows rapidly when the RPM is larger than 200.

Table 12. The volumetric flow rate through the final optimal turbine design at various RPMs.

RPM	Flow Rate (m^3/s)
50	0.1070
100	0.1106
150	0.1114
200	0.1129
250	0.1206
300	0.1317
350	0.1430
400	0.1553

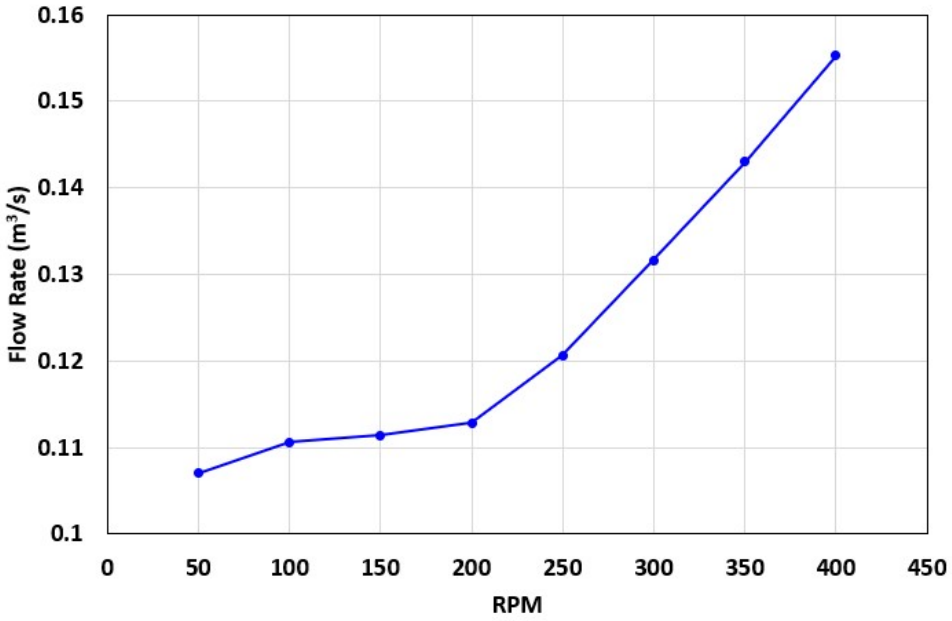

Figure 36. Volumetric flow rate through the final optimal turbine design at various RPMs.

7.2 Lesson Learned and Test Plan Deviation

In the present study, the overall Test Plan was followed. The project was well executed. ABS and HEC had monthly meetings to discuss findings and next steps. The project was completed by the deadline.

The only deviation from the original Test Plan was the omission of 30 cases during the stage of modifying the diffuser. We originally planned to evaluate a total of 108 cases (Table 1) for different diffuser geometries. We then realized that some changes in the diffuser geometry would not lead to increased power output based on results from the preceding stages. Instead of running through a set matrix of cases, we adopted a proactive search strategy: only the changes to the geometry that would reduce the obstruction of the turbine structures to the main flow would lead to an increased power output. Following

this new strategy, only 63 cases rather than 108 would have been needed for that stage. For a verification, we still added back 15 cases, which brough the total number of cases we ran for the diffuser to 78 (i.e., 30 cases omitted in the end). Both ABS and HEC agreed on this new search strategy and the reduction in the number of cases.

ABS also went beyond the original Test Plan. As requested by HEC, two extra cases that were not in the Test Plan were studied: (1) the hydrodynamic performance of the final optimal design but with a 4-bladed rotor and (2) the drag forces and coefficients on the entire turbine structures at two different incident current velocities for the final optimal design. The two extra case studies were beneficial to the present project and have strengthened our understanding of the current turbine performance. The results of the two case studies are summarized in Appendices 11.1 and 11.2, respectively.

8 Conclusions and Recommendations

CFD was used to evaluate the energy efficiency of different variates of HEC's baseline current turbine model. The shroud, the diffuser, and the hub of the baseline design were modified to create new variates. It was first determined that the 3-bladed baseline design had higher power output than its 4-bladed counterpart. For the 3-bladed configuration, the power output peaked at 200 RPM. For simplicity, the remaining parametric study was focused on rotors with three blades and a rotational speed of 200 RPM. Modifications to the original geometry was made for the shroud, the diffuser, and the hub in order, separately. An intermediate optimal design was identified for each stage. A final optimal design was reached after all three parts had been modified. It was found that the final optimal design had

- Three blades
- A shroud with a maximum camber reduced by 10%, a maximum camber location increased by 10%
- A diffuser with a maximum camber reduced by 10%, a maximum camber location increased by 10%, a thickness reduced by 10%, a diameter increased by 10%, and an expansion angle increased by 4 degrees
- A hub with a maximum camber reduced by 10% and a thickness reduced by 10%

compared to the baseline design. The final optimal design realized a 15% increase in the power output compared to the baseline design.

During the process of CFD analysis, a clear trend was observed: in order to increase power efficiency, one should attempt to reduce the flow blockage as much as possible. Specifically, the cross-sections of the shroud, the diffuser, and the hub should have small thicknesses, small cambers, and delayed maximum camber locations. For the diffuser, a diameter and a larger expansion will also help ease the obstruction of the structures to the incident flow.

The findings of this study will provide invaluable insight into the directions for design modification. This will further help with the setup of a more sophisticated energy efficiency optimization in the future phases of the development.

9 REFERENCES

[1] OpenFOAM User Guide: Cyclic Arbitrary Mesh Interface (AMI), https://www.openfoam.com/documentation/guides/v2112/doc/guide-bcs-coupled-cyclic-ami.html

[2] Morris, C., A. Mason-Jones, D. M. O'Doherty, and T. O'Doherty, The influence of solidity on the performance characteristics of a tidal stream turbine, Proceedings of the European Wave and Tidal Energy Conference, Nantes, France, September 6–11, 2015.

10 ACKNOWLEDGEMENTS

ABS gratefully acknowledges the financial support of TEAMER and very much appreciates the invaluable technical guidance provided by HEC.

11 APPENDIX

11.1 THE FINAL OPTIMAL DESIGN WITH 4-BLADED ROTOR

In this section, the hydrodynamic performance of the final optimal design with four blades instead of three (Figure 37) was evaluated as a confirmation that the 4-bladed series really would not be as efficient as their 3-bladed counterparts. The case setup and gridding remained consistent with those for all other cases except that the computational grids around the rotor blades were different. With four blades for the current case, it would be difficult to predict whether the power output would still peak at 200 RPM. We tested three different RPMs around 200, i.e., 150, 200, and 250.

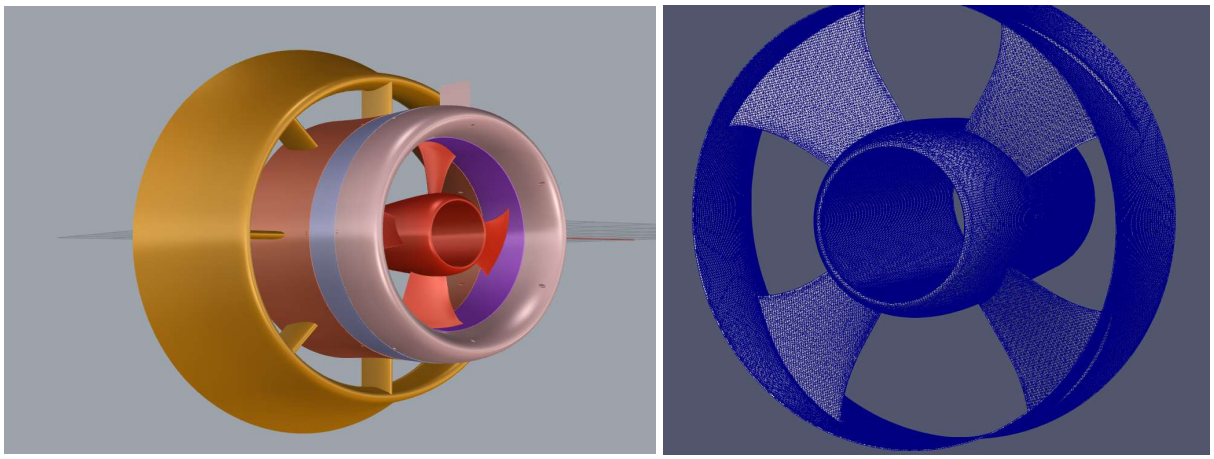

Figure 37. The final optimal design with a 4-bladed rotor (left) and the surface mesh on the rotor blades (right).

The torque and power values for the 4-bladed final optimal design, along with those for the 3-bladed final optimal design, are shown in Figure 38. It is confirmed that 200 RPM was still corresponding to the peak power output for the 4-bladed case. Table 13 summarized the output values of the torque and maximum power at RPM 200, showing the 10% difference between the two designs.

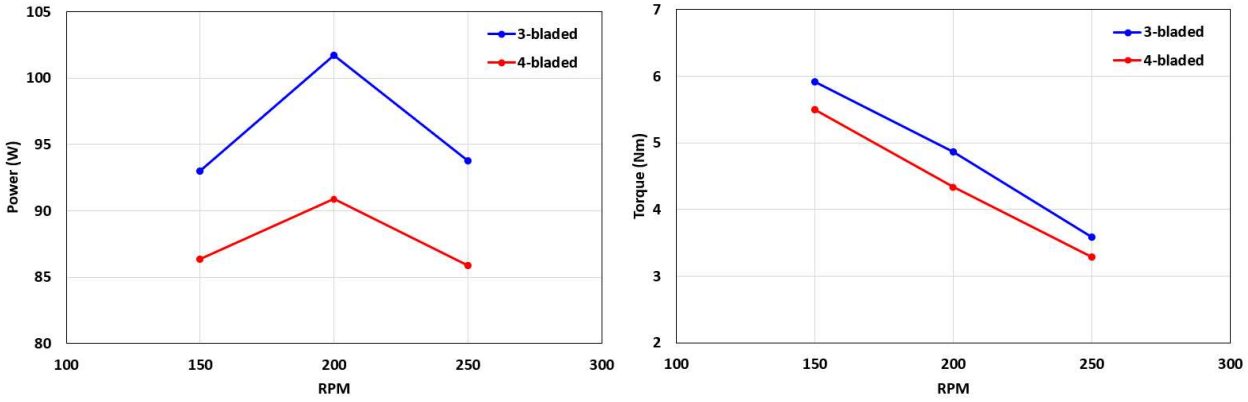

Figure 38. Torque (left) and power (right) values for the 3-bladed and the 4-bladed final optimal designs.

Table 13. The torque and power values of the 4-bladed and the 3-bladed final optimal design at RPM 200.

Number of blades	Torque (Nm)	Power (W)
4	4.34	90.90
3	4.86	101.73

Figures 39 and 40 show the patterns of the velocity component Ux in the plane at y = 0 as viewed from upstream and downstream, respectively. Figure 41 shows the dynamic pressure distribution in the plane at y = 0. Figure 42 presents the upstream and downstream views of the dynamic pressure distributions on the surfaces of the 4-bladed final optimal design of the current turbine.

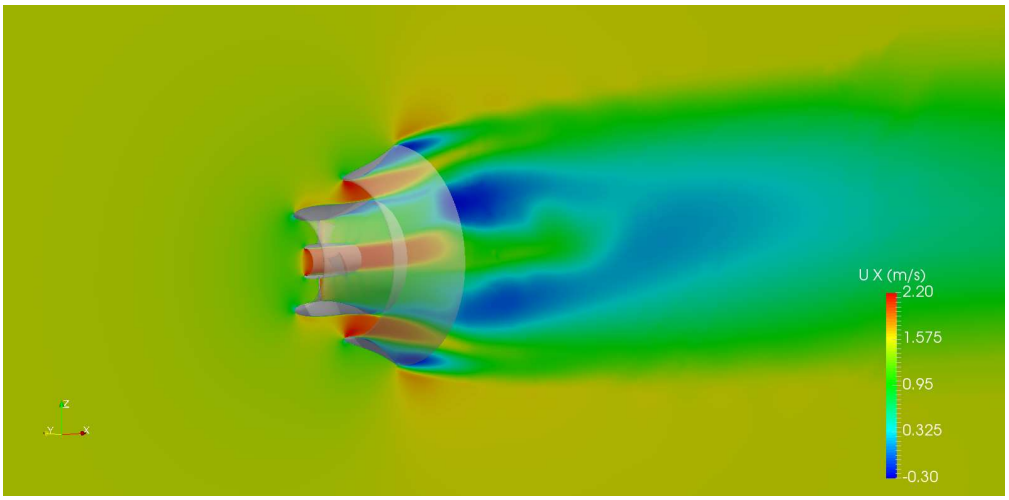

Figure 39. CFD-simulated velocity component Ux (viewed from upstream) for the 4-bladed final optimal design at y = 0 (RPM 200).

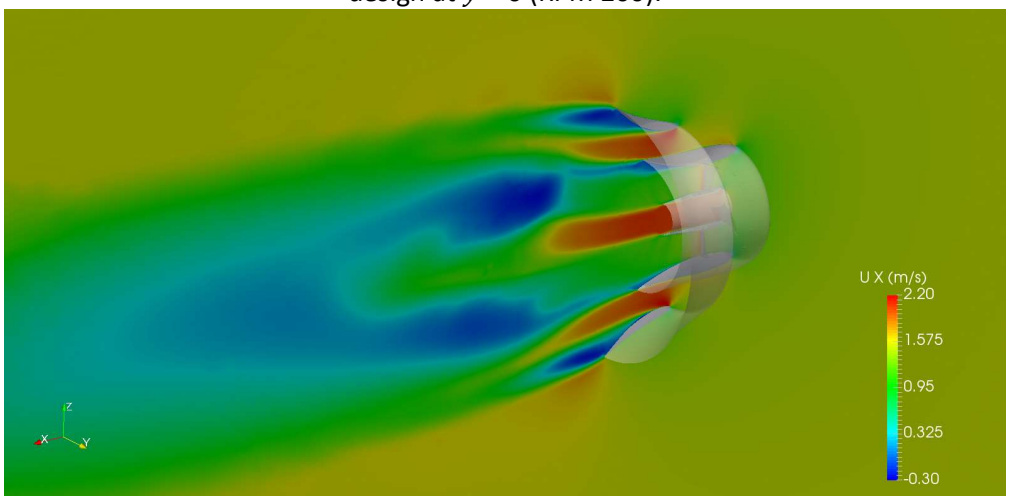

Figure 40. CFD-simulated velocity component Ux (viewed from downstream) for the 4-bladed final optimal design at y = 0 (RPM 200).

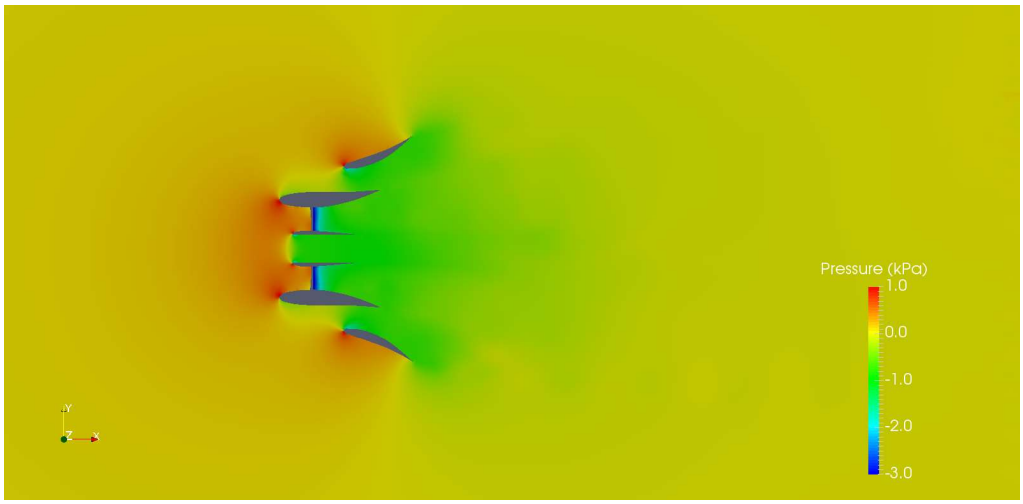

Figure 41. CFD-simulated dynamic pressure for the 4-bladed final optimal design at y = 0 (RPM 200).

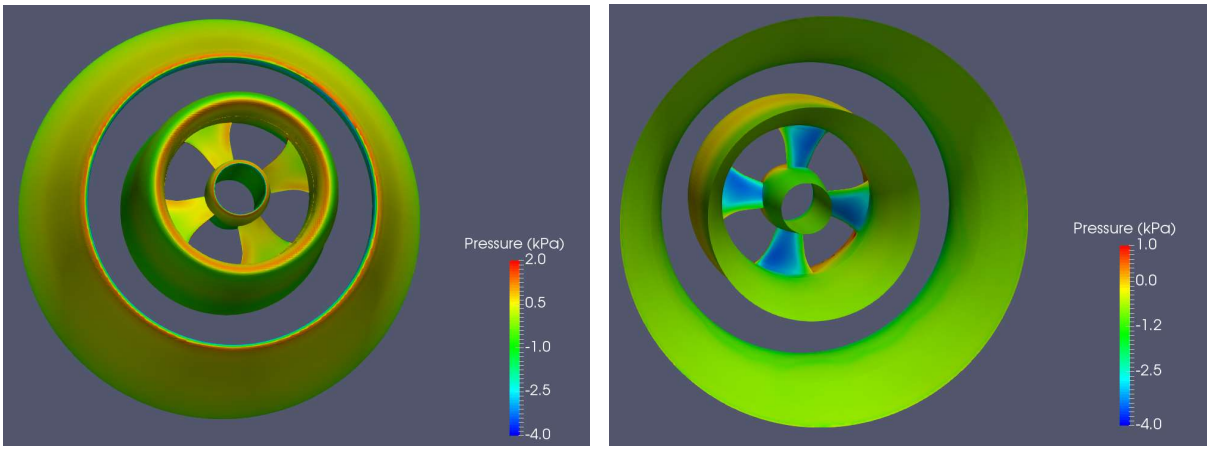

Figure 42. CFD-simulated dynamic pressure on the structural surfaces of the 4-bladed final optimal design (left: viewed from upstream; right: viewed from downstream; RPM 200).

11.2 Drag Forces on Current Turbine

The drag force is the total hydrodynamic force in the streamwise direction (i.e., the positive x direction) on all turbine structures as included in the present project. The drag coefficient, C_D, is commonly defined as

$$C_D = \frac{F_D}{\frac{1}{2}\rho A \ ^2} \tag{4}$$

where F_D is the drag force, ρ is the water density, V is the inflow velocity, and A denotes the rotor swept area as defined for Equations (1) and (2).

HEC requested two different inflow velocities, i.e., 1.5 and 2.5 m/s. Since results have been obtained for the case of 1.5 m/s, only a new CFD simulation was conducted for the case of 2.5 m/s at RPM 200. Both cases are based on the 3-bladed final optimal design.

Inflow Velocity of 1.5 m/s

The total drag force on the current turbine was decomposed into two components, i.e., the force on the rotor and the force on the stator. The force on the stator can be further decomposed into two sub-components: the part on the shroud and the part on the diffuser. Table 14 shows the different drag components as well as their respective percentages in the total drag. Figure 43 shows a pie-chart of the breakdown of the total drag to different components.

Table 14. The drag forces and drag coefficients for different structural components of the current turbine (the 3-bladed final optimal design with an inflow velocity of 1.5 m/s; RPM 200).

Component	Drag (N)	C_D	Percentage in the total drag (%)
Rotor	101.25	1.08	20.6
Shroud	73.61	0.79	15.0
Diffuser	315.69	3.38	64.4
Total	490.55	5.25	100

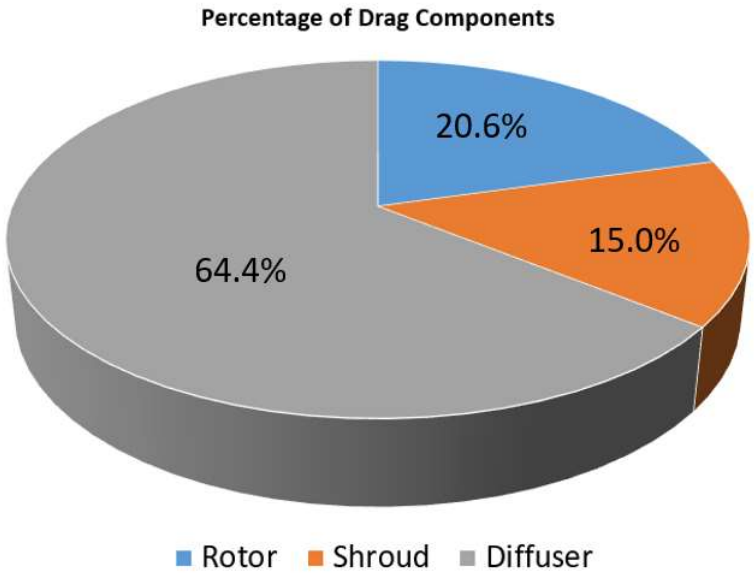

Figure 43. A breakdown of the total drag to different components (the 3-bladed final optimal design; inflow velocity 1.5 m/s; RPM 200).

Inflow Velocity of 2.5 m/s

The increased inflow speed was anticipated to increase the overall Reynolds number and hence affect the required grid sizes for resolving near-wall flows. We adjusted the computational grids by refining the rotor and stator meshes based on the new characteristic Reynolds number. The time-step was also reduced accordingly to 0.001 s. Other settings were kept the same as those for the final optimal design case for an inflow speed of 1.5 m/s.

Table 15 and Figure 44 show the total drag and drag coefficient and its breakdown to different components in a tabular and a graphical format, respectively.

Table 15. The drag forces and drag coefficients for different structural components of the current turbine (the 3-bladed final optimal design with an inflow velocity of 2.5 m/s; RPM 200).

Component	Drag (N)	C_D	Percentage in the total drag (%)
Rotor	309.39	1.19	22.1
Shroud	215.51	0.83	15.3
Diffuser	878.13	3.38	62.6
Total	1403.03	5.40	100

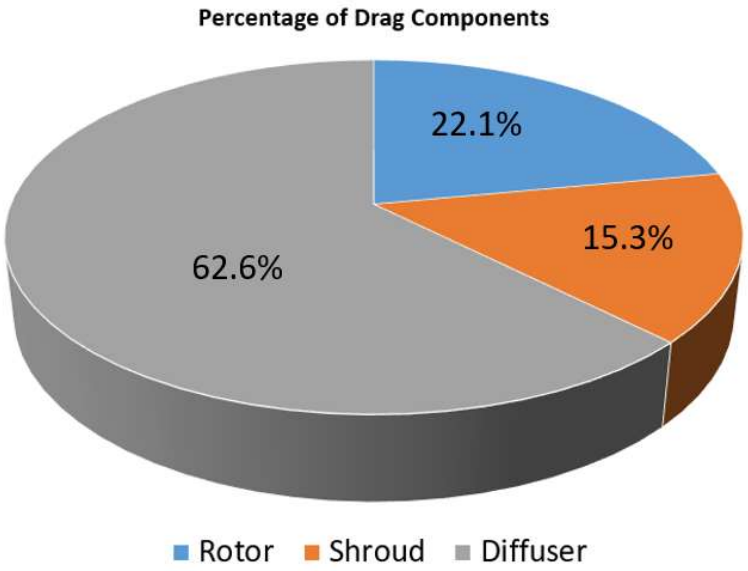

Figure 44. A breakdown of the total drag to different components (the 3-bladed final optimal design; inflow velocity 2.5 m/s; RPM 200).

From Figures 43 and 44, it can be observed that the breakdown of the drag components (i.e., the rotor, the shroud, and the diffuser) are quite consistent for both inflow velocities. The largest drag component resulted from the diffuser (more than 60%). Moreover, with the increasing inflow velocity, the rotor's share in the total drag also increased slightly (from 20.6 to 22.1%), but the stator's share decreased (from 79.4 to 77.9%).

Figures 45 and 46 show the Ux and dynamic pressure fields in the plane at y = 0 for the two inflow speeds (1.5 m/s and 2.5 m/s), respectively.

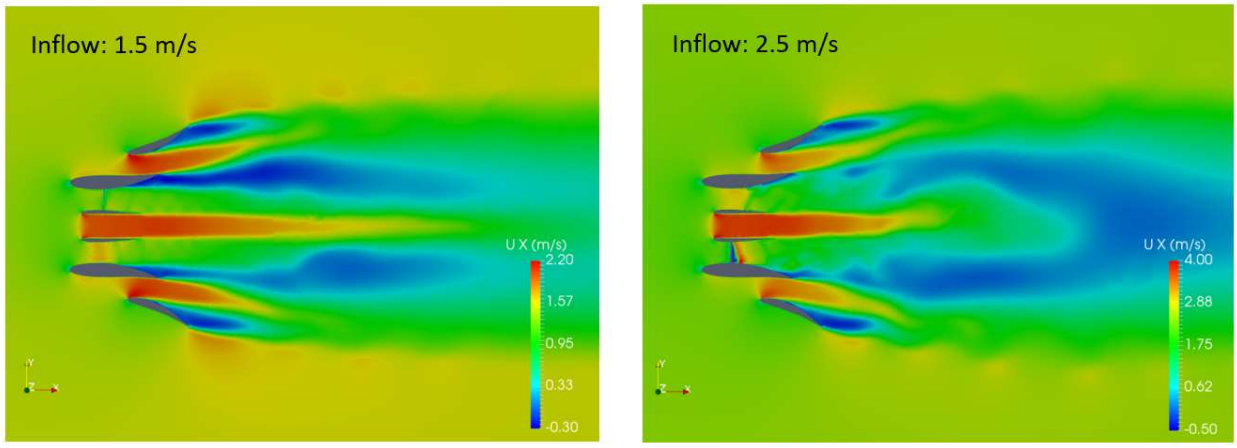

Figure 45. CFD-simulated velocity component Ux at y = 0 for the two inflow speeds (1.5 m/s and 2.5 m/s) for the 3-bladed final optimal design (RPM 200).

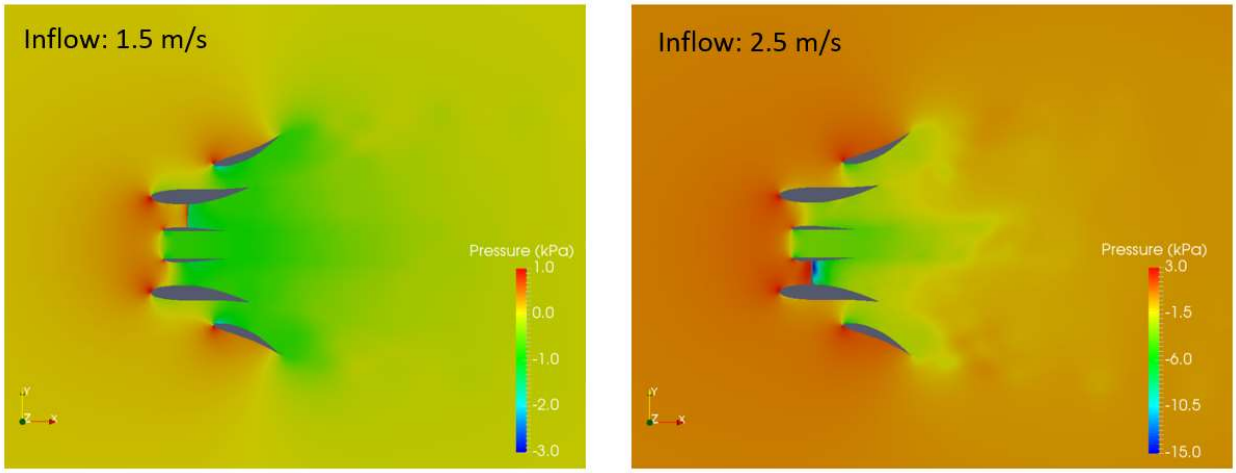

Figure 46. CFD-simulated dynamic pressure at y = 0 for the two inflow speeds (1.5 m/s and 2.5 m/s) for the 3-bladed final optimal design (RPM 200).

11.3 Convergence Tests of CFD Grids and Time-steps

The convergence tests for the time-step and grid-size were performed on a matrix of two different grid-size levels (fine and medium) by two different time-step levels (Δt = 0.001 s and Δt = 0.002 s) for the 3-bladed baseline design. The volume meshes for the computational domain and the surface meshes for the turbine structures are shown in Figures 47 and 48 for the medium and fine levels, respectively. The medium grid has a total cell number of 6.31 million, whereas the fine grid has 8.23 million cells.

The steady-state thrust and torque values were compared between the two sets of grids, as shown in Tables 16 and 17, respectively. It can be observed that the largest difference among all setups was less than 1.3%. Therefore, the medium grid and the time step of 0.002 s were chosen for all cases in this parametric study.

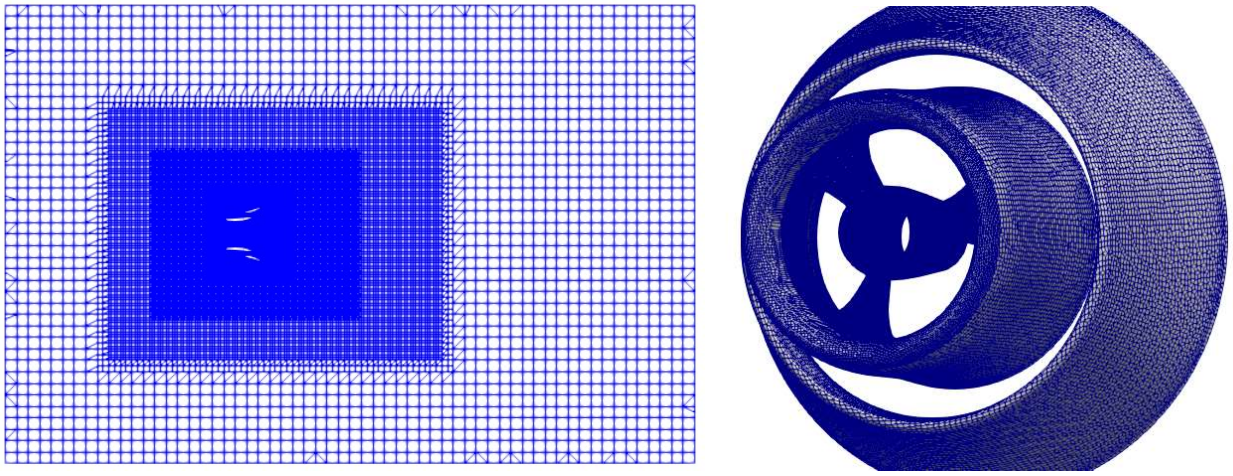

Figure 47. The medium grid for the baseline design (left: volume mesh at y = 0; right: surface mesh).

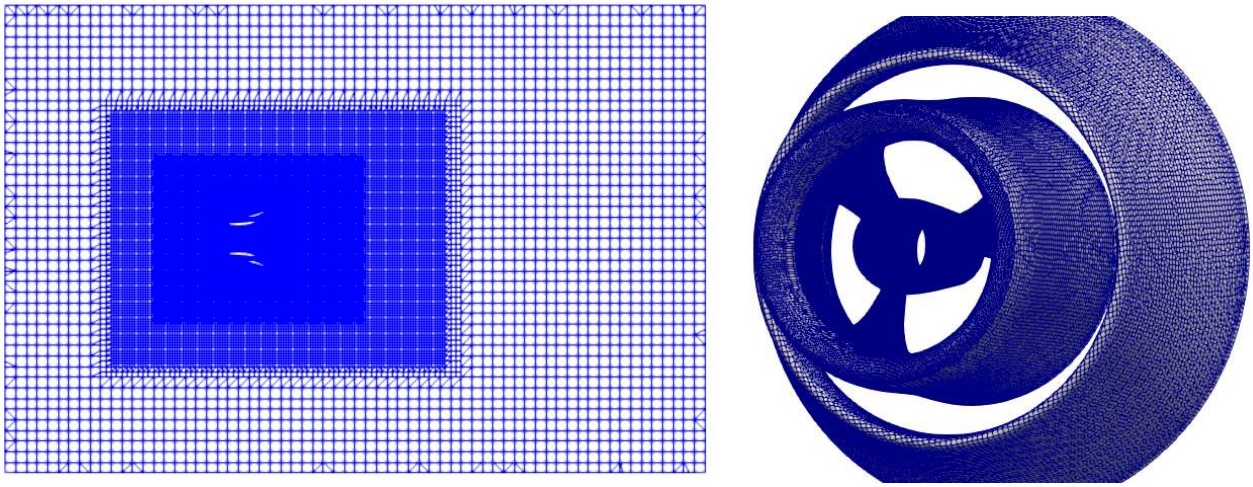

Figure 48. The fine grid for baseline design (left: volume mesh at y = 0; right: surface mesh).

Table 16. The differences in the calculated thrust value from using the two grids and two time-steps for the baseline design at RPM 200 and inflow velocity of 1.5 m/s.

Time-step	Medium Grid	Fine Grid
Δt = 0.001 s	-0.81%	0.89%
Δt = 0.002 s	0.0% (reference)	0.83%

Table 17. The differences in the calculated torque value from using the two grids and two time-steps for the baseline design at RPM 200 and inflow velocity of 1.5 m/s.

Time-step	Medium Grid	Fine Grid
Δt = 0.001 s	-1.16%	1.25%
Δt = 0.002 s	0.0% (reference)	1.12%